HHS Public Access

Author manuscript

Cell Rep. Author manuscript; available in PMC 2024 June 27.

Published in final edited form as:

Cell Rep. 2024 May 28; 43(5): 114143. doi:10.1016/j.celrep.2024.114143.

Dominant role for pigment epithelial CRALBP in supplying visual chromophore to photoreceptors

Marco Bassetto[1,2], **Alexander V. Kolesnikov**[3], **Dominik Lewandowski**[3], **Jianying Z. Kiser**[1,3], **Maximilian Halabi**[1], **David E. Einstein**[1,2], **Elliot H. Choi**[3], **Krzysztof Palczewski**[1,3,4,5], **Vladimir J. Kefalov**[1,3], **Philip D. Kiser**[1,2,3,6,7,*]

[1] Department of Physiology & Biophysics, University of California Irvine, Irvine, CA 92697, USA

[2] Research Service, Tibor Rubin VA Long Beach Medical Center, Long Beach, CA 90822, USA

[3] Department of Ophthalmology, University of California Irvine, Irvine, CA 92697, USA

[4] Department of Chemistry, University of California Irvine, Irvine, CA 92697, USA

[5] Department of Molecular Biology and Biochemistry, University of California Irvine, Irvine, CA 92697, USA

[6] Department of Clinical Pharmacy Practice, University of California Irvine, Irvine, CA 92697, USA

[7] Lead contact

SUMMARY

Cellular retinaldehyde-binding protein (CRALBP) supports production of 11-*cis*-retinaldehyde and its delivery to photoreceptors. It is found in the retinal pigment epithelium (RPE) and Müller glia (MG), but the relative functional importance of these two cellular pools is debated. Here, we report RPE- and MG-specific CRALBP knockout (KO) mice and examine their photoreceptor and visual cycle function. Bulk visual chromophore regeneration in RPE-KO mice is 15-fold slower than in controls, accounting for their delayed rod dark adaptation and protection against retinal phototoxicity, whereas MG-KO mice have normal bulk visual chromophore regeneration and retinal light damage susceptibility. Cone pigment regeneration is significantly impaired in RPE-KO mice but mildly impacted in MG-KO mice, disclosing an unexpectedly strong reliance of cone photoreceptors on the RPE-based visual cycle. These data reveal a dominant role for RPE-CRALBP in supporting rod and cone function and highlight the importance of RPE cell targeting for CRALBP gene therapies.

* Correspondence: pkiser@uci.edu.

AUTHOR CONTRIBUTIONS

M.B., K.P., V.J.K., and P.D.K. conceived and designed the research. M.B., A.V.K., M.H., J.K., D.E.E, D.L., and P.D.K. performed experiments. P.D.K. and M.B. wrote the initial draft and all authors contributed to and approved the final manuscript.

DECLARATIONS OF INTEREST: K.P. is a consultant for Polgenix Inc. and serves on the Scientific Advisory Board at Hyperion Eye Ltd. All other authors have declared that no conflict of interest exists.

INTRODUCTION

Image-forming vision is initiated by the photoactivation of rod and cone visual pigments within photoreceptor neurons. These visual pigments consist of an opsin protein component and a covalently linked 11-*cis*-retinaldehyde (11-*cis*-RAL) visual chromophore that converts to an all-*trans*-configuration upon absorption of light, triggering phototransduction.[1] Sustained vision requires the constant reverse isomerization of all-*trans*-RAL back to 11-*cis*-RAL, which occurs through multiple biochemical pathways.[2,3] The classical 'visual cycle', which is based in the retinal pigment epithelium (RPE), is the best-characterized pathway for the regeneration of 11-*cis*-RAL in the absence of light.[4] A separate light-independent regeneration system, located entirely within the neural retina, was reported to provide visual chromophore selectively to cone but not rod photoreceptors.[5,6] Finally, the RGR-photoisomerase regeneration system, which is active in both the RPE and Müller glia (MG), also supports 11-*cis*-RAL regeneration in a light-dependent fashion.[7–9]

After being produced by any of these regeneration systems, 11-*cis*-RAL is bound by cellular retinaldehyde-binding protein (CRALBP), which is encoded by the *Rlbp1* gene and expressed in both the RPE and MG.[10,11] This binding protein sequesters the reactive aldehyde away from non-physiological nucleophiles and prevents premature *cis-trans* photoisomerization.[12,13] CRALBP also facilitates 11-*cis*-retinoid production and likely plays a role in shuttling 11-*cis*-retinoids to appropriate subcellular compartments within the RPE and MG so they can be productively delivered to the photoreceptors.[7,13–15] As such, CRALBP is a linchpin molecule for efficient 11-*cis*-retinoid biosynthesis and photoreceptor function.

In humans, *RLBP1* mutations are associated with recessive retinal diseases that feature delayed dark adaptation, ERG abnormalities, subretinal lesions, and in some cases, photoreceptor degeneration leading to blindness.[16–18] To understand the molecular basis for these phenotypes, *Rlbp1*$^{-/-}$ knockout mice were generated and characterized.[19] They exhibit delayed dark adaptation and protection from light-induced retinal damage, which both originate from a slowing of 11-*cis*-RAL and rhodopsin regeneration following light exposure. However, because of the global disruption of *Rlbp1* in these mice, the relative contributions of CRALBP in RPE and MG to the observed phenotypes remained uncertain. Subsequent studies in *Rlbp1*$^{-/-}$ mice using viral restoration of *Rlbp1* expression in the RPE or MG[20] as well as gene knockdown/knockout studies in larval zebrafish[21–23] were performed, but these studies have produced conflicting results. Moreover, rod-specific functions were generally not investigated in these studies.

To address this knowledge gap, we generated mouse strains that allow timed knockout of *Rlbp1* selectively in the RPE or MG and examined these mice for defects in 11-*cis*-RAL biosynthesis and photoreceptor function. By deleting *Rlbp1* after the retina is fully formed, we avoided potential developmental abnormalities allowing the collection of data that directly reflect CRALBP physiology.[20] Our results reveal a dominant role for RPE-expressed CRALBP in support of both rod and cone photoreceptor physiology.

RESULTS

Generation of high-efficiency, cell-specific CRALBP knockout mice –

To silence *Rlbp1* expression in the RPE or MG, we employed tamoxifen-inducible LoxP-Cre recombinase technology. First, we generated a floxed *Rlbp1* mouse line to enable Cre recombinase-mediated exon six deletion, thereby generating a null allele (Figure S1A). We confirmed the susceptibility of the floxed locus to Cre-mediated recombination *in vitro* using a multiplexed PCR-based assay (Figure S1B and Table S1). We then crossed floxed *Rlbp1* mice with two different Cre driver lines: the *GLAST-CreER* line (*GLAST-Cre*), which expresses tamoxifen-inducible Cre in Müller glia[24], and the $Rpe65^{CreERT2}$ line (*Rpe65-Cre*), which expresses tamoxifen-inducible Cre in the RPE.[25] These lines were generated on backgrounds in which the gene encoding the α subunit of rod transducin (*Gnat1*) was either in wild-type form ($Gnat1^{+/+}$) or deleted ($Gnat1^{-/-}$), the latter enabling selective study of cone photoresponses.

Next, we induced *Rlbp1* knockout in $Rlbp1^{F/F}$ $GLAST\text{-}Cre^{+}$ and $Rlbp1^{F/F}$ $RPE65\text{-}Cre^{+/-}$ mice by treating the animals with tamoxifen to activate Cre starting at post-natal day (P) 21 and P30, respectively. Tamoxifen was administered either by intraperitoneal (IP) injection for 5 consecutive days or in the chow diet for three weeks. Afterward, the animals were maintained until 3 months of age before assessing CRALBP expression levels. CRALBP was eliminated from the RPE cell layer in the *RPE65-Cre* line while inner retinal staining was comparable to genotype-/age-matched controls (Figure 1A–D). MG-CRALBP knockout was also highly efficient, although sparse residual CRALBP-positive MG were observed (Figure 1E–H). We further quantified KO efficiency by performing Western blots on isolated neural retina and RPE from the two mouse lines. RPE-CRALBP was undetectable in tamoxifen-treated $Rlbp1^{F/F}$ $Rpe65\text{-}Cre^{+/-}$ mice, while neural retina (*i.e.,* MG) expression was comparable between tamoxifen-treated and control mice (Figure S2A–D). MG-CRALBP was reduced to ~6.9% of vehicle controls (range: 2.5 – 12.5%) in $Rlbp1^{F/F}$ $GLAST\text{-}Cre^{+}$ mice treated with tamoxifen chow whereas RPE expression was comparable between the two groups (Figure S2E–H). MG-CRALBP expression was also strongly reduced with the IP tamoxifen administration method, although with more variability (range: 5.3 – 46.5% as compared to controls) relative to the chow delivery method (Figure S2I–L). Therefore, we employed Western blotting throughout the study to exclude the animals with sub-optimal MG-CRALBP knockout from analysis. Together, these data demonstrate robust and targeted CRALBP knockout in the two different mouse lines and exclude major compensatory changes in CRALBP expression in the opposing cell type. Henceforth, we refer to tamoxifen-treated $Rlbp1^{F/F}$ $Rpe65\text{-}Cre^{+/-}$ mice as RPE-CRALBP KO and tamoxifen-treated $Rlbp1^{F/F}$ $GLAST\text{-}Cre^{+}$ mice as MG-CRALBP KO.

Cell-specific CRALBP knockout does not perturb retinal structure –

We next examined retinal structure in each mouse line at three months of age. Spectral-domain optical coherence tomography (OCT) measurement of the outer nuclear layer (ONL) thickness, representing the area occupied by photoreceptor nuclei, did not reveal significant differences between tamoxifen-treated and control groups (Figure S3A–H). Retinal cryo-sections showed similar M- and S-cone opsin localization in MG-CRALBP

and RPE-CRALBP KO mice as compared to controls of the same age and genotype (Figure S4). Faint M-cone opsin immunofluorescence was observed in the outer plexiform layer and outer nuclear layer of RPE-CRALBP KO mice suggestive of opsin mislocalization (Figure S4, **white arrowheads**). Similarly, *Rlbp1*$^{-/-}$ mouse cryosections showed some M-cone opsin signal in the outer plexiform and outer nuclear layers, suggesting M-cone opsin mislocalization as observed previously[20] (Figure S4), as well as a reduced number of M-cones, whereas S-cone opsin and S-cone number were comparable among the lines. We quantified the cone photoreceptor density in each mouse line by staining retinal flatmounts with M- and S-cone antibodies (Figure 2A). This analysis confirmed a significantly lower M-cone density in *Rlbp1*$^{-/-}$ mice compared to the control lines (Figure 2B) whereas the cell-specific knockout lines did not differ from controls. There were also no significant differences in S-cone density among the groups (Figure 2C).

Dark-adapted cone photoreceptor but not rod photoreceptor responses are suppressed in RPE-CRALBP KO mice –

To assess whether the photoreceptor electrophysiology of cell-specific CRALBP KO mice exhibits baseline defects, we recorded dark-adapted ERGs on mice with wild-type *Gnat1* and *Gnat1*$^{-/-}$ backgrounds. No significant differences were observed in the dark-adapted, rod-driven b-wave (Figure 3A,B) or a-wave (Figure S5A,B) intensity-response functions or implicit times (Figure S5C–F) between the knockout and control groups on a wild-type *Gnat1* background for either mouse line, indicating normal dark-adapted rod phototransduction and synaptic transmission. However, we found that M-cone b-wave responses were notably suppressed in *Gnat1*$^{-/-}$ RPE-CRALBP KO mice compared to age-/genotype-matched controls despite 24 h of dark adaptation (Figure 3C). This suppression was reflected in a 4-fold increase in the half-saturating stimulus intensity ($I_{1/2}$) between RPE-CRALBP KO mice and control mice, resembling the 2-or-3-fold dark-adapted sensitivity reduction observed for *Rlbp1*$^{-/-}$ *Gnat1*$^{-/-}$ mice.[26] Despite the sensitivity reduction, maximal responses were comparable between the two groups. Conversely, cone ERG b-wave responses in MG-CRALBP KO mice were indistinguishable from control mice (Figure 3D). These data indicated a dependence of cone photoreceptors on RPE-CRALBP for maintenance of their photoresponses and suggested that the suppressed dark-adapted ERG b-wave responses observed in *Rlbp1*$^{-/-}$ *Gnat1*$^{-/-}$ mice are linked to the absence of CRALBP in the RPE as opposed to the MG.[20,26]

RPE-CRALBP KO severely impacts bulk visual chromophore regeneration –

Next, we examined the impact of CRALBP deficiency in the RPE and MG on bulk visual chromophore synthesis following a strong photobleach. For these experiments, animals were dark-adapted and then exposed to bright light sufficient to bleach ~95% of the visual pigment in the retina. The animals were then placed in the dark to allow visual pigment recovery for defined periods after which ocular retinoids were quantified by HPLC. The recovery of 11-*cis*-RAL in these experiments directly reflects the regeneration of visual pigments (primarily rhodopsin).[27,28] Representative HPLC traces for KO mice as well as genotype/age-match controls are shown in Figure 4. In comparison to control animals, recovery of 11-*cis*-RAL was markedly impaired in RPE-CRALBP KO mice (Figure 4A). By two hours after the photobleach, RPE-CRALBP KO mice regenerated only ~10% of

their 11-*cis*-RAL, whereas control animals had fully recovered (Figure 4B). Concomitantly, the RPE-CRALBP KO mice showed severely delayed clearance of all-*trans*-retinyl esters as compared to controls, indicating an impairment in the isomerohydrolase step of the visual cycle (Figure 4C). However, Western blot analysis excluded a direct role for RPE65 isomerohydrolase downregulation in the RPE-CRALBP KO mice as a factor contributing to the visual cycle delay (Figure S6). We note that all-*trans*-retinyl esters were significantly lower in dark-adapted RPE-CRALBP KO mice than in controls, like what was observed for *Rlbp1*$^{-/-}$ mice (Figure 4C).[18] By 24 to 48 h after the photobleach, levels of 11-*cis*-RAL and all-*trans*-retinyl esters had returned to their starting dark-adapted levels, demonstrating that RPE-CRALBP is not essential for the rhodopsin regeneration process but does strongly influence its rate.[18,19] By contrast, no significant differences in retinoid metabolism were found when comparing MG-CRALBP KO mice to controls (Figure 4D–F).

To quantity the rates of 11-*cis*-RAL recovery in the experimental groups, we fit the recovery data (Table S2 and Methods S1) with the rate-limited model of visual pigment regeneration[29]. Least-squares fits to the data are shown in Figure S7. The best-fit lines showed a 15.5-fold lower V_{max} for the RPE-CRALBP KO mice as compared to controls, while K_m was comparable between the groups (Table S3). By contrast, V_{max} for MG-CRALBP KO and controls were within 5% of each other. Notably, the initial slope values ($v_o = \frac{V_{max}}{1 + K_m}$) we obtained for the Cre-positive control animals were comparable to published values for wild-type mice (Table S3).[29] The delay in visual chromophore synthesis in the RPE-CRALBP KO mice was similar in magnitude to the delay (10- to 15-fold slower regeneration) observed in *Rlbp1*$^{-/-}$ mice[19], but in both models, 11-*cis*-RAL eventually reaches the dark-adapted level. By contrast, CRALBP deletion in MG had little or no detectable effect on bulk visual chromophore synthesis. The higher V_{max} observed for the MG-CRALBP control mice versus the RPE-CRALBP control mice is consistent with the known greater RPE65 activity in the former lines (*i.e.,* two vs one copy of wild-type Leu450 RPE65).[30,31]

To further evaluate the impact of CRALBP deficiency within the RPE on rod photoreceptor physiology, we measured recovery of scotopic ERG responses following a deep photobleach in RPE-CRALBP KO and control mice (Figure 5). The ERG responses of control mice recovered significantly at 60 min post-illumination, and both a- and b-waves fully recovered within 180 min. By contrast, RPE-CRALBP KO mice failed to recover measurable ERG a- and b-wave responses even after 180 min of dark adaptation. These data revealed a profound influence of RPE-CRALBP on the rate of rod dark adaptation and further demonstrated that the rod dark adaptation impairment shown previously for *Rlbp1*$^{-/-}$ mice[19] arises from the loss of CRALBP expression in the RPE.

RPE-CRALBP KO but not MG-CRALBP KO protects against acute retinal damage induced by bright light –

Rlbp1$^{-/-}$ mice were reported to be protected against light-induced retinal damage.[19] We investigated the relative importance of MG- and RPE-CRALBP in mediating this effect (Figure 6). Near-complete loss of photoreceptors, as reflected by destruction of the ONL band, and retinal detachment were observed for every line except RPE-CRALBP KO

mice, which exhibited a retinal structure indistinguishable from non-light exposed animals (Figure S3). The retinal structure disruption was associated with the presence of abundant autofluorescent spots in the retina indicative of photoreceptor lesions. This data established that RPE-CRALBP rather than MG-CRALBP modulates the susceptibility of the mouse retina to light damage. This result is congruent with the slowed rhodopsin regeneration in RPE-CRALBP KO mice, which is known to protect against retinal light damage.[32]

RPE-CRALBP KO impairs M-cone dark adaptation following a brief bleaching light exposure –

To examine the impact of cell-specific CRALBP deletion on cone pigment regeneration, we measured the recovery of ERG b-wave dim flash responses after an acute photobleach in RPE-CRALBP KO and MG-CRALBP KO mice on a *Gnat1*$^{-/-}$ background.[33] These responses reflect the level of retinal photosensitivity, which is a physiologic proxy for visual pigment regeneration specifically in cone photoreceptors.[6] Specifically, we calculated the recovery of M-cone b-wave flash sensitivity (S_f) from the linear portion of the intensity-response function.

Dark recovery of M-cone ERG b-wave sensitivity was significantly suppressed in RPE-CRALBP KO mice as compared to controls (Figure 7A,B). Flash sensitivity was reduced about two-fold in RPE-CRALBP KO as compared to control mice starting at 12.5 min after the start of dark adaptation, and the reduction was sustained for the duration of the recording period. This level of flash sensitivity reduction is comparable to that observed for *Rlbp1*$^{-/-}$ mice, suggesting a major contribution of RPE-CRALBP deficiency to the phenotype.[26] By contrast, dark recovery of M-cone sensitivity was indistinguishable between MG-CRALBP KO mice and controls (Figure 7C,D). Thus, M-cone visual chromophore recovery following an acute bleach, like bulk visual chromophore recovery, was strongly dependent on the RPE pool of CRALBP.

A role for MG-CRALBP in M-cone photoreceptor dark-adaptation is unmasked by an extended bleaching light exposure –

The lack of an effect of MG-CRALBP knockout on M-cone ERG sensitivity recovery was surprising given previous studies showing a role for this pool of CRALBP in cone function.[20,26] Recently, CRALBP was shown to facilitate visual chromophore synthesis through the RGR photoisomerase system.[7] Thus, we considered the possibility that the impact of MG-CRALBP deficiency could be more readily detected during and after an extended light exposure that constantly bleaches the visual pigment at a high rate and simultaneously engages the RGR-based regeneration system.[34]. Figure 7E shows the raw flash sensitivity data for MG-CRALBP knockout and control animals. We observed a significantly greater M-cone b-wave desensitization for the MG-CRALBP KO mice as compared to control animals during both the period of illumination and the subsequent dark recovery period. These differences were accentuated in the normalized data due to the slightly higher dark-adapted sensitivity in the MG-CRALBP KO mice compared to controls (Figure 7F). Specifically, the normalized MG-CRALBP KO S_f values fluctuated between ~50–75% of control values during both the light exposure and subsequent dark adaptation periods. For comparison, the published normalized S_f values for MG-RGR

knockout mice were ~75–97% and 50–80% of control mice during the extended light exposure and subsequent dark recovery periods, respectively.[34] These results indicate that MG-CRALBP contributes to M-cone dark adaptation following more extreme bleaching conditions, although its role is comparatively minor relative to RPE-CRALBP, which strongly influenced M-cone dark recovery even after a brief bleaching light exposure (Figure 7A,B).

Absolute quantification of CRALBP levels in RPE and MG –

It was previously suggested that MG-CRALBP could serve as a storage pool for rapidly deliverable visual chromophore to cone photoreceptors in mice.[35] Although CRALBP levels have been individually quantified in bovine RPE and neural retina[36], levels in the mouse neural retina and RPE are unknown. To determine the size of this potential storage pool in the mouse eye, we quantified CRALBP levels in the RPE and neural retina of both pigmented (C57BL/6J) and albino (BALB/cJ) mice. Per eye absolute quantification was achieved by Western blot using known masses of recombinantly expressed *Mus musculus* CRALBP (Table S4, Figure S8A–H). The levels of CRALBP in the two strains were comparable, with ~1–1.6 pmol of CRALBP per eyecup (*i.e.,* RPE) and 2.5–2.8 pmol per neural retina (*i.e.,* MG) (Figure S8I). The bovine eye was reported to contain ~0.7–1 nmol of CRALBP in the RPE and ~1–2 nmol of CRALBP in the neural retina.[36,37] Thus, the RPE:MG CRALBP expression ratio in the mouse eye is comparable to that of the bovine eye but the overall expression level differs by about three orders of magnitude. Based on differences in rhodopsin content (25 nmol/eye vs 500 pmol/eye in bovine and mouse, respectively), we estimate that the mouse eye contains about 20 times less CRALBP than the bovine eye when normalized based on rhodopsin mass. Assuming ~10–15 pmol of cone opsin per mouse retina[38], we estimate a ~0.3–0.4 molar ratio of total CRALBP to total cone opsin. This sub-stoichiometric pool of CRALBP-bound 11-*cis*-retinoids helps explain the dependence of mouse cones on CRALBP-facilitated enzymatic production of 11-*cis*-RAL within the RPE.[26]

DISCUSSION

The landmark study describing the phenotypes in *Rlbp1*$^{-/-}$ mice provided long-sought confirmation of the physiological importance of CRALBP in visual function.[19] However, the roles of the CRALBP protein pools found in the RPE and MG in supporting photoreceptor physiology remained incompletely defined. The *Rlbp1* conditional knockout mouse lines described here allowed us deconvolute the contributions of each CRALBP cellular pool to the phenotypes observed in *Rlbp1*$^{-/-}$ mice.[25] Specifically, we found that loss of RPE-localized CRALBP exclusively underlies the dramatic (~15-fold) slowing of visual chromophore synthesis and accumulation of retinyl esters, the delayed rod dark adaptation, and the protection against light-induced retinal degeneration found in *Rlbp1*$^{-/-}$ mice. Moreover, our physiological studies of cell-specific CRALBP KO lines generated on a *Gnat1*$^{-/-}$ background revealed a strong dependence of M-cone photoreceptors on the RPE pool of CRALBP for efficient dark adaptation. By contrast, the MG pool plays a subsidiary role, possibly by supporting the RGR-based regeneration system[34], that is discernable only under prolonged bleaching and subsequent recovery in the dark. Notably, we excluded the

possibility of incomplete MG-CRALBP knockout as a cause for the weak cone phenotype by using data from mice where complete or near-complete CRALBP deletion in the neural retina was confirmed by Western blotting. Although the dependence of cones on RPE-based visual chromophore biosynthesis runs contrary to the original notion that cones are supported by a non-classical visual cycle pathway that is independent of the RPE[5,39,40], it is fully consistent with more recent work showing an important role for the RPE in the maintenance of cone photoresponses.[26,35,41,42]

We observed a significant delay in the processing of all-*trans*-retinyl esters formed after an acute bleaching light exposure in RPE-CRALBP KO mice. The same observation in *Rlbp1*$^{-/-}$ mice led to the proposal that apo-CRALBP functions immediately downstream of the isomerohydrolase (RPE65) to accept nascent 11-*cis*-retinol and facilitate its oxidation to 11-*cis*-RAL[19,43]. This idea was supported by the ability of CRALBP to facilitate 11-*cis*-retinol synthesis by isomerohydrolase *in vitro*.[14] Based on more recent structural and biochemical data, we propose that apo-CRALBP instead directly accepts 11-*cis*-RAL from RDH5. In the setting of RPE-CRALBP knockout, the inefficient sequestration of 11-*cis*-RAL slows the turnover rate of RDH5 leading to an accumulation of 11-*cis*-retinol that exerts product inhibition on RPE65.[44] It is this product inhibition that causes a delay in the clearance of all-*trans*-retinyl ester substrates of RPE65. The residual 11-*cis*-RAL that is produced by RDH5 in the absence of CRALBP retains the ability to traffic to the photoreceptor outer segment, albeit at a much lower rate. Additionally, our finding that basal retinyl ester stores are depleted in RPE-CRALBP KO mice compared to age-/genotype-matched controls (Figure 4A,C) suggests that CRALBP may protect against retinoid loss from the RPE.

Some prior data have suggested a key role for MG-CRALBP in cone function, which requires reconciliation with our current results. Initial studies in zebrafish larvae employing a morpholino knockdown indicated complementary and equally important roles for MG- and RPE-CRALBP pools for the function of cones.[21,23] However, a recent study using *rlbp1a*$^{-/-}$ (expressed in RPE) and *rlbp1b*$^{-/-}$ (expressed in MG) larval zebrafish indicated a much stronger role for RPE-CRALBP in cone photoreceptor function[22], like the results we obtained here. Gene-restoration studies in mice have also suggested that the MG play a dominant role in some aspects of cone photoreceptor function.[20] We note that the experiments in which cone function was restored by MG-selective but not RPE-selective gene delivery were performed with isolated neural retina, where the RPE cells are omitted from the experiment. When cone ERG b-wave flash sensitivities were recorded *in vivo*, it was found that viral-mediated *Rlbp1* cDNA delivery to either cell type was sufficient to partially rescue the dark adaptation delay found in *Rlbp1*$^{-/-}$ mice. However, the level of CRALBP expression in the rescued lines was not quantitated in this study, making it possible that overexpression in the MG could lead to a supraphysiologic effect. Also, the absence of *Rlbp1* during development may have altered the retina in such a way that cones developed a greater ability to utilize MG-derived retinoids. Thus, the different outcomes could derive from the different starting points of the retina – one in which retinoid flow was perturbed throughout the retinal development process and another in which the disruption was triggered post-development.

If MG-CRALBP plays no role in rod photoreceptor function and is of limited importance in cone photoreceptor function, what other physiological role(s) could it subserve? It was reported that *Rlbp1*$^{-/-}$ mice have impaired pupillary light reflexes, which are driven in part by intrinsically photosensitive retinal ganglion cells (ipRGCs) that express the invertebrate-like pigment, melanopsin.[20] This non-image forming pigment, like rod and cone pigments, requires 11-*cis*-RAL chromophore. Because MG span almost the full thickness of the retina, it was hypothesized that CRALBP in the MG could help transport 11-*cis*-retinoids from the RPE to the ipRGCs.[45] Indeed, later experiments showed that prolonged melanopsin photoresponses are impaired in the setting of *Rlbp1* deletion in the MG and a subset of RPE cells. Thus, the role of MG-CRALBP in non-image-forming vision could be more significant than its role in supporting cone photoreceptor function.

Finally, the data we present have implications for the treatment of *RLBP1*-associated retinopathies and therapeutics. Because the phenotypes observed in RPE-CRALBP KO mice account for many or all of the rod- and cone-phenotypes observed in *Rlbp1*$^{-/-}$ mice, our results support the development of *RLBP1*-gene augmentation strategies targeting RPE cells. Specifically, our work highlights the applicability of the subretinal injection method already being used clinically to target the RPE for the treatment of Leber congenital amaurosis [46] and supports the approach used in an *RLBP1* gene therapy trial. Similarly, our data suggest that the development of gene editing approaches aimed at correcting loss-of-function mutations in *RLBP1* should prioritize RPE cell targeting. The protection from acute retinal damage induced by bright light in RPE-CRALBP KO mice suggests that slowing the visual cycle by targeting RPE-CRALBP may have therapeutic significance as previously suggested from studies of humans heterozygous for *RLBP1* loss-of-function mutations.[18]

Limitations of the study –

This study focused on dissecting the physiological contributions of the RPE- and MG-CRALBP pools to the regeneration of rod and cone visual pigments in a rod-dominant mammal. It remains possible that MG-CRALBP could play a more prominent role in cone visual pigment regeneration in cone-dominant mammals or in the cone-rich foveal/macular region of the primate retina. Although our study provides further support for repetitive rhodopsin photobleaching enabled by visual chromophore recycling within the RPE as the key mediator of acute light-induced retinal degeneration, it did not address the underlying molecular mechanism of the damage, specifically whether the photoreceptor degeneration is caused directly by all-*trans*-retinal released by photoactivated rhodopsin or rather by bisretinoid condensation products formed from retinaldehyde and phospholipid. Finally, although we did not observe significant structural changes within the retinas of *Rlbp1* conditional knockout mice at the times points examined, it remains possible that retinal pathology could manifest at later time points as previously observed in aged *Rlbp1*$^{-/-}$ mice.[18]

STAR METHODS

RESOURCE AVAILABILITY

Lead Contact—Further information and requests for resources and reagents should be directed to and will be fulfilled by the lead contact, Philip D. Kiser (pkiser@uci.edu).

Materials Availability—Newly generated materials from this study are available upon reasonable request. *Rlbp1* floxed mice described in this paper are being deposited with Jackson Laboratory (Stock No. 039407)

Data and Code Availability

- All data supporting the findings of this study are available from the corresponding author upon reasonable request.
- The R code used in this study is included in the supplemental information file.
- Any additional information required to reanalyze the data reported in this paper is available from the lead contact upon request.

EXPERIMENTAL MODEL AND STUDY PARTICIPANT DETAILS

Study approvals.—All animal procedures were approved by the Institutional Animal Care and Use Committees (IACUC) at the University of California Irvine and the Tibor Rubin VA Long Beach Medical Center. All experimental protocols were conducted following the *NIH Guide for the Care and Use of Laboratory Animals*, the recommendations of the American Veterinary Medical Association Panel on Euthanasia, and the Association for Research in Vision and Ophthalmology (ARVO) *Statement for the Use of Animals in Ophthalmic and Visual Research.*

Animal husbandry.—Animals were housed in a standard 12/12-h light/dark cycle environment, fed a standard soy protein-free rodent chow diet (Envigo Teklad 2020X, except for experiments involving tamoxifen chow induction), provided water *ad libitum*, and housed in plastic cages with standard corncob rodent bedding and 6 g nestlets (Ancare).

Generation of the floxed *Rlbp1* mouse line.—Generation of the floxed *Rlbp1* mouse line was performed by Ingenious Targeting Laboratory using standard techniques under a fee-for-service contract. Briefly, iTL BF1 embryonic stem cells were electroporated with a targeting construct to introduce LoxP sites flanking exon 6 of the *Rlbp1* gene as well as an frt-flanked neomycin (Neo) cassette to allow clonal selection. The targeting construct long homology arm extended ~6.2 kb upstream of the distal LoxP sequence while the short homology arm (SA) extended ~ 2.3 kb downstream from the Neo cassette. The positioning of the distal LoxP site as well as the Neo cassette was carefully chosen to avoid interference with potential regulatory elements. Targeted stem cells were selected with neomycin and clones were then expanded for PCR screening. The Neo cassette was deleted during colony expansion through the action of FLP recombinase. Properly targeted stem cells were microinjected into BALB/c blastocysts. The resulting chimeras with a high-percentage black coat color were mated to wild-type C57BL/6N mice to generate germline

Neo cassette-deleted offspring, which were further mated with wild-type C57BL/6N and C57BL/6J mice to eliminate the FLP transgene and rd8 mutation.[47] The resulting mice were used for subsequent downstream breeding.

Generation of mouse lines for conditional knockout studies.—Homozygous floxed *Rlbp1* (*Rlbp1*$^{F/F}$) mice were crossed with *Gnat1*$^{-/-}$ mice[33] and the resulting offspring were in-crossed to produce *Rlbp1*$^{F/F}$ *Gnat1*$^{+/+}$ and *Rlbp1*$^{F/F}$ *Gnat1*$^{-/-}$ mice. These lines were then crossed with *Rpe65-Cre* mice[25] or *GLAST-Cre* mice (JAX stock # 012586) to produce *Rlbp1*$^{F/F}$ *Rpe65-Cre*$^{+/-}$ and *Rlbp1*$^{F/F}$ *GLAST-Cre*$^{+}$ mice on either a *Gnat1* wild-type or *Gnat1*$^{-/-}$ background. Because current genotyping methods do not distinguish zygosity for the *GLAST-Cre* transgene, we only specify the presence of the transgene as *GLAST-Cre*$^{+}$. All lines were confirmed by PCR to be free of the rd8 mutation. The *GLAST-Cre* lines were homozygous for the Leu450 variant of RPE65 while the *Rpe65-Cre* mice were heterozygous for the Leu450 variant of RPE65, the other CreERT2-fused copy of *Rpe65* being the Met450 variant.[25] Standard PCR-based genotyping protocols for all of the loci mentioned above are specified in Table S1. Cre recombinase activity was induced by IP injection of tamoxifen (Sigma-Aldrich, T5648) dissolved in corn oil vehicle (10–20 mg/mL stock) for five consecutive days (1 mg for three days, then 2 mg for two days) or by feeding mice a tamoxifen-loaded chow diet (250 mg tamoxifen/kg chow, Envigo, TD.130856) for three weeks. Tamoxifen treatment was started at either P21 (*GLAST-Cre* mice) or P30 (*Rpe65-Cre* mice). These two regimens produced comparable results in the *Rpe65-Cre*$^{+/-}$ mice while a greater occurrence of strongly MG-CRALBP-deleted animals (*i.e.,* with > 90% knockout efficiency) was observed for the chow delivery method in *GLAST-Cre*$^{+}$ mice. Control mice received either corn oil vehicle IP or standard chow, depending on the tamoxifen administration method employed. Approximately equal numbers of male and female mice were used for experiments.

METHOD DETAILS

Genotyping procedures.—Mouse ear punch samples were digested overnight at 55 °C in 150 μL of DirectPCR(tail) buffer (Viagen) containing proteinase K (Viagen) at a concentration of 4 μg/mL. Proteinase K was inactivated by incubating at 95 °C for 1 h. The supernatant was then used for standard PCR-based genotyping using GoTaq® Green Master Mix (Promega) and a Bio-Rad T100 thermal cycler. Primers and cycling parameters used for each region of interest are shown in Table S1. PCR reactions were analyzed by agarose gel electrophoresis. For in vitro Cre recombinase assays, genomic DNA from the experimental mice was incubated with purified Cre recombinase according to the manufacturer instructions (New England Biolabs, M0298). Following heat inactivation of the Cre enzyme, the resulting DNA was used as a PCR template as described in Table S1.

Recombinant CRALBP production and quantification.—A pET3a plasmid encoding *Mus musculus* CRALBP with an *N*-terminally fused 6-histidine tag was produced by Genscript. The plasmid was transformed into chemically competent T7 express cells (New England Biolabs). Transformants were selected on LB plates containing 100 μg/mL ampicillin. Five to ten individual colonies were inoculated into LB media containing 100 μg/mL ampicillin and grown at 37 °C with constant shaking until an OD_{600} of 0.5 was

measured. The temperature was then lowered to 27 °C and the culture was allowed to incubate overnight with continuous shaking to allow for constitutive expression to occur. The bacteria cells were then pelleted by centrifugation and resuspended in 20 mM HEPES-NaOH, pH 7.2, containing 0.1 M NaCl (buffer A). The resuspended cells were lysed in a French press and the lysate was centrifuged at >100,000*g* for 40 min at 4 °C. The resulting supernatant was collected and applied to 1 mL of Ni-NTA resin (Qiagen) pre-equilibrated with 20 mM HEPES-NaOH, pH 7.2, 0.5 M NaCl, and 10 mM imidazole-HCl, pH 7.2 (buffer B). The column was washed with 10 column volumes of buffer B and the bound protein was eluted with 20 mM HEPES-NaOH, pH 7.2, 0.5 M NaCl, and 300 mM imidazole-HCl, pH 7.2. Fractions were analyzed by SDS-PAGE, and those containing CRALBP were pooled and buffer-exchanged into buffer A containing 1 mM DTT using a 10 kDa MWCO Amicon (Millipore). The sample was then applied to a 1 mL hydroxyapatite column (Bio-Rad) pre-equilibrated with buffer A, which was washed with 10 column volumes of buffer A. The protein was eluted with a linear gradient of buffer A containing 0 to 200 mM sodium phosphate, pH 7.2. Fractions containing CRALBP were pooled, concentrated, and applied to a pre-equilibrated 25 mL Superdex 200 Increase gel filtration column. The protein was eluted with buffer A and fractions containing CRALBP were pooled, concentrated, and stored at −80 °C until further use. The sample was subjected to quantitative amino acid analysis (Table S4) allowing experimental determination of its molar extinction coefficient ($\varepsilon_{280\ nm}$ = 24972.1 $M^{-1}{\cdot}cm^{-1}$) and absolute CRALBP mass (Texas A&M University, Protein Chemistry Laboratory).

***In vivo* visual chromophore recovery assays and HPLC analysis.—**Fifteen min prior photobleaching, the pupils of the mice were dilated by administration of a drop of 1% tropicamide ophthalmic solution to the eye (Somerset Therapeutics, LLC, NDC code: 70069–0121-01) under a dim-red safety light and the animals were maintained in the dark for an additional 15 min. The mice were then exposed to 10,000 lux white light for 10 min to bleach their visual pigment. One set of animals was immediately euthanized, their eyes enucleated, transferred into dry ice, covered with aluminum foil, and kept in the dark (0 h time point). The rest of the mice were allowed to recover in the dark for various periods before euthanasia and eye collection. For retinoid analysis, both eyes from each animal were homogenized in 1 mL of 10 mM sodium phosphate buffer, pH 8.0, containing 50% v/v methanol (Sigma–Aldrich; 34860–1L-R) and 100 mM hydroxylamine, pH = 8 (Sigma-Aldrich; 159417–100G). After a 15 min incubation at room temperature, 2 mL of 3 M sodium chloride were added to the homogenate. The resulting sample was extracted twice with 3 mL of ethyl acetate (Fisher Scientific; E195–4). The combined organic phase was dried *in vacuo* and reconstituted in 450 μL hexane. Retinoids extracts (100 μL) were analyzed with an Agilent 1260 Infinity II HPLC system equipped with a diode array detector (DAD) and a Zorbax Sil column (5 μm; 4.6 mm × 250 mm; Agilent Technologies). The mobile phase consisted of 0.6% v/v ethyl acetate in hexanes (Fisher Scientific; H302–4) flowing at 1.4 mL/min for 17 min followed by a step increase to 10% v/v ethyl acetate in hexanes flowing at 1.4 mL/min for an additional 25 min. Retinoids were detected by monitoring absorbance at 325 nm and 360 nm with continuous spectral recording. Peaks were identified based on their absorbance spectra and retention times relative to authentic

standards. Absolute quantification of retinoids was conducted by peak integration with reference to authentic retinoid standards.

Kinetic analysis of 11-*cis*-RAL recovery.—Visual chromophore recovery data were fit with the rate-limited recovery model:[29,48]

$$11cRAL(t) = 11cRAL(max) \times \left(1 - K_m{*}W_p[\frac{BFr}{K_m} \times exp\left(\frac{BFr - V_{max}{*}t}{K_m}\right)]\right)$$

where $11cRAL(t)$ is the time-dependent recovery of 11-*cis*-RAL, $11cRAL$(max) is the maximal level of 11-*cis*-RAL after complete dark adaptation, K_m is the semi-saturation constant, V_{max} is the maximal rate of pigment regeneration, BFr is the fraction of 11-*cis*-RAL bleached during light exposure, and W_p is the principal branch of the Lambert W function. $11cRAL$(max) and BFr were obtained directly from the data while V_{max} and K_m were estimated by non-linear regression. $11cRAL$(max) was fixed at the averaged value of the final time point of the recovery, where the progress curve had plateaued, while BFr was fixed at [1 – 11cRAL(0 min)]. Non-linear regression was carried out in R v.4.2.1 within R studio using nlsLM within the minpack.lm package. The Lambert W function was evaluated using the LambertWp function within the pracma package. For the RPE-CRALBP KO mice and controls, both K_m and V_{max} were treated as adjustable parameters. For the MG-CRALBP KO mice and controls, V_{max} was adjustable whereas K_m was fixed at 0.2 to stabilize the non-linear regression, as described previously.[48] Fits were also generated with a simple exponential recovery model, but these were significantly less satisfactory compared to fits using the rate-limited model according to the corrected Akaike information criterion (AICc).

Western blotting.—Mice were euthanized by CO_2 asphyxiation and their eyes enucleated. The anterior segment was dissected and discarded. The neural retina was removed by dissection, taking care to avoid detachment of the underlying RPE, and collected into a tube that was placed on dry ice. The eye cup was placed into a separate tube which was placed on dry ice. Samples were stored at −80 °C until needed. At that point, samples were placed on ice and ice-cold 1X PBS containing 1X protease inhibitors (Bimake) was added at a volume of 300 μL for the retina sample and 250 μL for the eyecup sample. The samples were lysed by 4 cycles of sonication (5 sec on, 5 sec off, at 50% amplitude) conducted in a cold room. The samples were then centrifuged at 22,000*g* for 15 min at 4 °C to separate the soluble and insoluble material. The soluble fractions were collected and used for CRALBP Western blotting. The pellet was then placed in 200 μL of 1X PBS containing 1% SDS and 1X protease inhibitors (Bimake) and sonicated as described above except for 6 cycles. The material was then centrifuged at 22,000*g* for 15 min at 4 °C to separate solubilized from insoluble material. The solubilized material was collected for RPE65 Western blotting. Twenty μL of solubilized material was added to 6 μL of SDS-PAGE loading buffer and the sample was incubated at room temperature for 10–15 min. The sample was then centrifuged and 4–15 μL of the soluble portion was loaded onto a 10 or 12% SDS-PAGE gel. After electrophoresis, the proteins were transferred onto a prewetted 0.45 um PVDF membrane using a Bio-Rad semi-dry transfer system. The membrane was immediately blocked in 5% milk in PBST for 60 min. For CRALBP

analyses, a rabbit anti-CRALBP antibody (UW55)[15] was diluted 1:2000 in PBST containing 5% non-fat milk. Mouse anti-α-tubulin (Abcam, ab7291) or anti-β-actin (Abcam, ab6276) antibodies were also added at a 1:5000 dilution for use as loading controls. The antibody mixture was incubated with the membrane for 16 h at 4 °C with gentle rocking. For RPE65 analyses, an anti-RPE65 antibody (KPSA1)[49] and a rabbit anti-β-actin antibody (Abcam, ab8227) were diluted 1:100 and 1:5000, respectively, in PBST containing 5% non-fat milk, and the antibody mixture incubated with the membrane for 24 h at 4 °C with gentle rocking. The membrane was then washed three times with 5 mL of 1X PBST. Then goat anti-rabbit IgG (LICOR, 926–32211) and donkey anti-mouse IgG (LICOR, 926–68072) secondary antibodies were premixed at a 1:5000 dilution with 5 mL of 5% milk in PBST and then added to the membrane. The incubation was conducted at room temperature for 1 h with gentle rocking. Then the membrane was washed three times with PBST, placed in 1X PBS, and imaged with a LICOR imaging system. For quantitative CRALBP Western blotting, retina and RPE supernatant fractions were prepared from *Rlbp1*$^{-/-}$ mice as described above. Purified CRALBP was then added to the supernatant fractions to produce a stock that was further serially diluted into the supernatants to achieve the desired concentrations of CRALBP. This procedure was performed to account for masking effects as previously described.[31] Further sample preparation was performed as described above for the experimental CRALBP samples. Western blot image contrast and coloring were globally adjusted using Adobe Illustrator or Adobe Photoshop software. Band intensities were quantified using ImageJ software.[50] CRALBP or RPE65 signals were then normalized to those of the loading controls.

Retinal cryo-sectioning and immunohistochemistry.—Following euthanasia, mouse eyes were enucleated and placed in 1x PBS. A puncture was made at the limbus using a 23-gauge needle and the eye was then placed in 1x PBS containing 4% (w/v) paraformaldehyde (Sigma-Aldrich) for 15 min at room temperature to fix the tissue. The eye was placed back into 1x PBS and the anterior segment was removed by dissection. The resulting eyecup was fixed for an additional 15–30 min at room temperature. After fixation, the eyecups were sequentially incubated at room temperature in 1x PBS containing 5%, 10%, and 20% (w/v) sucrose (MilliporeSigma) for 30 min at each concentration. The eyecups were then transferred into a 1:1 mixture of 30% sucrose and O.C.T. compound (Fisher Scientific) and incubated overnight at 4 °C. The next day, the eyes were embedded in the same 30% sucrose/O.C.T. mixture and frozen on top of a dry ice-chilled metal block. Retinal sections were cut at a thickness of 10 μm at −20 °C using a Leica CM1850 cryostat and stored at −80 °C until needed. The retinal sections were rehydrated with 1x PBS and then blocked and permeabilized for 30 min with 0.2% (v/v) Triton X-100 (Millipore Sigma) and 5% normal goat serum (Abcam) in 1x PBS. The sections were then incubated overnight with anti-CRALBP primary antibody (1:1000, UW55), anti-M-cone opsin primary antibody (1:250, Novus, NB110–74730), or anti-S-cone opsin antibody (1:250, Novus, NBP1–20194) in a solution containing 0.2% Triton X-100 and 5% normal goat serum in 1x PBS. The sections were washed with 1x PBS 3 times, and then incubated with Alexa Fluor 594-conjugated goat anti-rabbit IgG (1:250; Thermo-Fisher Scientific, A11037) in 1x PBS. The sections were then washed with 1x PBS 5 times and mounted with VECTASHIELD Mounting Medium containing DAPI (Vector Laboratories) for imaging.

Fluorescence and bright-field images were acquired with a Keyence BZ-X800 All-in-One fluorescence microscope. Image contrast and coloring were globally adjusted using Adobe Illustrator or Adobe Photoshop software.

M and S cone staining and quantification on retina flatmounts.—The retinal flatmounts were prepared as described previously[51] from *Rlbp*$^{-/-}$ *Gnat1*$^{-/-}$ mice fed a standard chow diet as well as *Rpe65-Cre*$^{+/-}$ *Rlbp1*$^{F/F}$ and *GLAST-Cre*$^{+}$ *Rlbp1*$^{F/F}$ mice fed with tamoxifen-containing or standard chow diet (controls). Mice, aged 3–5 months, were euthanized by CO_2 asphyxiation and cervical dislocation. Eyes were enucleated post-mortem with the superior position marked on the cornea and fixed in 4% paraformaldehyde (PFA) in 1x PBS for 50 min. After fixation, the eyes were washed three times with 1x PBS, each time for 5 min, and then dissected on a microscope slide, removing the optic nerve and cornea, followed by puncturing the center of the cornea with a 25-gauge needle. Cohan-Vannas spring scissors (Fine Science Tools) were used to cut off the cornea, make four symmetric radial incisions, and mark the superior position by cutting a small triangular cut. The lens and vitreous were removed, and the eyecups were oriented with the sclera side facing up. After gently removing the sclera-RPE-choroid layer, the retinas were transferred to a 24-well plate containing 1x PBS. Next, the PBS was removed, and retinas were permeabilized and blocked with 1x PBS containing 1% Triton X-100 and 5% donkey serum (Millipore Sigma, #S30–100ML) for 1 h at room temperature (RT). To stain cone photoreceptors, the buffer was replaced with 1x PBS containing 0.5% Triton X-100, 5% donkey serum, and rabbit M-opsin or S-opsin polyclonal antibodies (1:500; Novus, NB110–74730 or NBP1–20194, respectively). After 64–72h incubation with primary Abs, retinas were washed three times each time for 10 min in PBST buffer (1x PBS with 0.5% Triton X-100) and then incubated for 2 h at RT with secondary antibodies (donkey polyclonal anti-rabbit, Alexa Fluor 488, #A21206, Fisher Scientific) at dilutions of 1:500 in PBST containing 5% donkey serum. Retinas were washed three times for 10 min with PBST and then twice with 1x PBS. Finally, retinas were mounted with a non-hardening Vectashield medium (#H-1900; Vector Labs) and protected with coverslips. The retinas were imaged within 1–3 days after mounting using a Keyence BZ-X800 microscope (Keyence Corp.) equipped with a 20x objective lens and a GFP filter (exposure 1/5 sec, +6dB, 40–60 Z-stacks) by collecting between 4,500 – 8,500 images for each retina. The M-cone densities were quantified by averaging the number of cones from four areas (240 × 180 μm each) in the superior, inferior, nasal, and temporal retina quadrant at 0.7 – 1 mm from the optic nerve. The S-cone densities were quantified similarly across the nasal and inferior retina quadrants. Cone outer segments in the coded images were then quantified by a blinded investigator via manual counting.

***In vivo* retinal imaging.—**Mice were anesthetized by an IP injection of ketamine (100 mg/kg) and xylazine (8.75 mg/kg) and pupils were dilated with 1% tropicamide and 10% phenylephrine before imaging. Ultrahigh-resolution spectral domain OCT (Bioptigen, Research Triangle Park, NC) was performed for cross-sectional imaging of mouse retinas as described previously.[52] Briefly, five frames of OCT images were first acquired in the B-mode in two orthogonal directions and then averaged. Images were then analyzed using ImageJ software. Briefly, for each animal, the images collected from each eye were used

to measure the thickness of the outer nuclear layer (ONL) in the four retinal quadrants at 0.5 mm from the optic nerve head. The values from the right and left eye of the same animal were averaged. During the same session, the fundus was imaged by scanning laser ophthalmoscopy (SLO) (Heidelberg Engineering, Heidelberg, Germany) in autofluorescence mode as previously described.[52]

Light damage experiments.—Before light damage experiments, mice (3–5-months-old on a *Gnat1* wild-type background) were dark-adapted for 48 hours. Pupils were dilated by the application of a drop of 1% atropine sulfate to the eye (Ophthalmics Inc.). The mice were placed in a cage with a light-reflective white coating. Each cage was divided into four equal compartments with transparent Plexiglas separators. To prevent grouping and consequent light shielding, single animals were placed into their own compartment for the duration of the experiment. Mice were exposed to broad-spectrum 15,000 lux white light emitted by clusters of LEDs placed on top of each white cage for 8 hours. The animals had full access to food and water during light exposure. During the light exposure, atropine sulfate was applied to mouse eyes every two hours to maintain mydriasis. After light exposure, animals were returned to their normal cages and kept under standard lighting conditions for one week before SLO and OCT imaging.

***In vivo* ERG intensity-response measurements.—**Mice were dark-adapted either overnight in the case of *Gnat1*$^{-/-}$ used for M-cone ERG recordings or for 48 h in the case of *Gnat1* wild-type mice used for rod ERG recordings. All procedures were performed under a dim-red safety light. The mice were anesthetized using a cocktail of ketamine (100 mg/kg) and xylazine (4 mg/kg). Pupils were dilated by application of a drop of 1% atropine sulfate to the eye. Mouse body temperature was maintained at 37°C with a heating pad. Full-field ERG responses to calibrated green (530 nm) LED light delivered within a Ganzfeld bowl were recorded from both eyes by contact corneal electrodes held in place by a drop of Gonak solution (Akorn). ERGs were recorded using a clinical ERG setup (UTAS Bigshot, LKC Technologies) adapted for mice. The b-wave intensity-response data obtained from *Gnat1*$^{-/-}$ mice were fit with the Naka-Rushton equation:

$$A = \frac{A_{max} \cdot I^n}{I^n + I_{1/2}^n}$$

where A is the transient-peak response amplitude, A_{max} is the maximal response amplitude, I is the flash intensity, n is the Hill coefficient, and $I_{1/2}$ is the half-saturating light intensity. A Q value of 1% was used to detect and exclude outlier data points from the non-linear regression fitting.[53]

***In vivo* ERG measurement of rod dark adaptation.—**Before ERG recording, mice on a wild-type *Gnat1* background were dark-adapted for 48 h. Under a red safety light, the mice were anesthetized by isoflurane inhalation and their pupils were dilated with topical administration of 1% tropicamide ophthalmic solution (Akorn; 17478–102-12) and 10% phenylephrine ophthalmic solution (MWI Animal Health #054243), followed by 0.3% hypromellose (Akorn; 9050–1) to maintain corneal hydration. Anesthetized mice were

placed on a heated pad set to 37 °C to prevent hypothermia. ERG responses were measured using a Diagnosys Celeris rodent-ERG device (Diagnosys LCC, Lowell, MA, USA). Ocular stimulator electrodes were placed on the corneas, the reference electrode was positioned subdermally between the ears, and a ground electrode was placed in the rear leg. The eyes were subjected to a green-light stimulus (peak emission 544 nm, bandwidth ~160 nm) of 0.1 cd·s/m^2, which exclusively excites rod photoresponses. The responses obtained from 3 consecutive stimuli with an inter-stimulus interval of 30 sec were averaged, and the a- and b-wave amplitudes were acquired from the averaged ERG waveform. Data were analyzed with Espion V6 software (Diagnosys LLC). Using this method, scotopic-ERG responses were measured first from dark-adapted animals. Next, the same animals were placed in a white cage and exposed to 10,000 lux white light for 5 min. The animals were then placed back in the dark and rod-driven ERG responses were recorded at 5 min, 1 h, 2 h, and 3 h after the bright light exposure to track the dark adaptation process.

***In vivo* ERG measurement of cone dark adaptation.—**Mice on *Gnat1*$^{-/-}$ background were dark-adapted overnight and then anesthetized by IP injection of a ketamine and xylazine solution (100 mg/kg and 4 mg/kg, respectively). Pupillary mydriasis was produced with a drop of 1% atropine sulfate applied to the eye. The animals were placed on a 37 °C heating pad to prevent hypothermia. ERG responses were measured from both eyes by contact corneal electrodes held in place by a drop of Gonak solution. Full-field ERGs were recorded with the UTAS BigShot apparatus (LKC Technologies) using a range of test flashes of calibrated green 530-nm LED light delivered within a Ganzfeld bowl. M-cone ERG b-wave flash sensitivity (S_f) was calculated from the linear part of the intensity-response based on the following equation:

$$S_f = \frac{A}{A_{max} \cdot I}$$

where A is the cone b-wave dim flash response amplitude (in μV), A_{max} is the maximal response amplitude for that retina (in μV), and I is the flash strength (in cd·s/m^2). Sensitivity was first determined under dark conditions for each eye and normalized to the maximum cone ERG b-wave amplitude obtained with the brightest white light stimulus delivered by the xenon flash tube (700 cd·s/m^2).

Two different protocols were employed. In the first one, cone S_f recovery was monitored after an acute, near-complete (> 90%) bleach of cone pigment by a 35-sec exposure to 520-nm bright LED light focused on the surface of the cornea. The M-cone opsin bleaching fraction was estimated by the following equation:

$$F = 1 - e^{(-I \cdot P \cdot t)}$$

where F is the fraction of pigment bleached, t is the duration of the light exposure (s), I is the bleaching light intensity of 520-nm LED light (1.3×10^8 photons/μm/s), and P is the photosensitivity of mouse M-cones at the wavelength of peak absorbance (7.5×10^{-9} μm^2, adopted from [57]).

In the second protocol, bright green background Ganzfeld illumination (300 cd/m^2; estimated to bleach dark-adapted M-cone pigment at a rate of 0.8%/sec) was applied continuously for 60 min while the M-cone b-wave S_f was monitored at periodic intervals. Two additional doses of ketamine (~30% of the initial dose each) were applied in the middle and at the end of the illumination period, respectively, and a small drop of PBS solution was gently applied to the eyes with a plastic syringe as needed, to protect them from drying and maintain electrode contacts. After the 60-min illumination period, the recovery of cone ERG b-wave S_f was followed in darkness for up to 30 min.

QUANTIFICATION AND STATISTICAL ANALYSIS

No statistical methods were applied to predetermine sample size. The ages of mice used for experiments are given in the figure legends. Except for M- and S-cone counting from retina flatmounts, the experiments were not randomized, and the investigators were not blinded to allocation prior to data analysis. Statistical analyses and graph generation were carried out using GraphPad Prism or R studio. Statistical methods and details of descriptive statistics are provided in the figure legends. A P value of less than 0.05 was considered significant.

Supplementary Material

Refer to Web version on PubMed Central for supplementary material.

ACKNOWLEDGMENTS

This research was supported in part by grants from the Department of Veterans Affairs (I01BX004939 to P.D.K.), the National Eye Institute (R01EY034519 to P.D.K. and K.P., R01EY009339 to K.P., and R01EY030912 to V.J.K.), a Research to Prevent Blindness Career Advancement Award (to P.D.K.), Knights Templar Eye Foundation Career Starter Awards (to M.B. and D.L.), and an International Retina Research Foundation Postdoctoral Award (to M.B.). The authors acknowledge support from NIH grant P30EY034070 and from an unrestricted grant from Research to Prevent Blindness to the Gavin Herbert Eye Institute at the University of California, Irvine. The contents of this publication do not necessarily represent the official views of any funding agency.

REFERENCES

1. Wald G (1968). The molecular basis of visual excitation. Nature 219, 800–807. [PubMed: 4876934]
2. Kiser PD, Golczak M, and Palczewski K (2014). Chemistry of the retinoid (visual) cycle. Chem. Rev. 114, 194–232. 10.1021/cr400107q. [PubMed: 23905688]
3. Kiser PD, and Palczewski K (2020). Pathways and disease-causing alterations in visual chromophore production for vertebrate vision. J. Biol. Chem. 296, 100072. 10.1074/jbc.REV120.014405. [PubMed: 33187985]
4. Wright CB, Redmond TM, and Nickerson JM (2015). A History of the Classical Visual Cycle. Prog. Mol. Biol. Transl. Sci. 134, 433–448. 10.1016/bs.pmbts.2015.06.009. [PubMed: 26310169]
5. Mata NL, Radu RA, Clemmons RC, and Travis GH (2002). Isomerization and oxidation of vitamin a in cone-dominant retinas: a novel pathway for visual-pigment regeneration in daylight. Neuron 36, 69–80. [PubMed: 12367507]
6. Wang JS, Estevez ME, Cornwall MC, and Kefalov VJ (2009). Intra-retinal visual cycle required for rapid and complete cone dark adaptation. Nat. Neurosci. 12, 295–302. nn.2258 [pii]10.1038/nn.2258. [PubMed: 19182795]
7. Zhang J, Choi EH, Tworak A, Salom D, Leinonen H, Sander CL, Hoang TV, Handa JT, Blackshaw S, Palczewska G, et al. (2019). Photic generation of 11-cis-retinal in bovine retinal pigment epithelium. J. Biol. Chem. 294, 19137–19154. 10.1074/jbc.RA119.011169. [PubMed: 31694912]

8. Chen P, Hao W, Rife L, Wang XP, Shen D, Chen J, Ogden T, Van Boemel GB, Wu L, Yang M, and Fong HK (2001). A photic visual cycle of rhodopsin regeneration is dependent on Rgr. Nat. Genet. 28, 256–260. 10.1038/90089. [PubMed: 11431696]

9. Morshedian A, Kaylor JJ, Ng SY, Tsan A, Frederiksen R, Xu T, Yuan L, Sampath AP, Radu RA, Fain GL, and Travis GH (2019). Light-Driven Regeneration of Cone Visual Pigments through a Mechanism Involving RGR Opsin in Muller Glial Cells. Neuron 102, 1172–1183 e1175. 10.1016/j.neuron.2019.04.004. [PubMed: 31056353]

10. Sparkes RS, Heinzmann C, Goldflam S, Kojis T, Saari JC, Mohandas T, Klisak I, Bateman JB, and Crabb JW (1992). Assignment of the gene (RLBP1) for cellular retinaldehyde-binding protein (CRALBP) to human chromosome 15q26 and mouse chromosome 7. Genomics 12, 58–62. [PubMed: 1733864]

11. Bunt-Milam AH, and Saari JC (1983). Immunocytochemical localization of two retinoid-binding proteins in vertebrate retina. J. Cell Biol. 97, 703–712. [PubMed: 6350319]

12. Saari JC, and Bredberg DL (1987). Photochemistry and stereoselectivity of cellular retinaldehyde-binding protein from bovine retina. J. Biol. Chem. 262, 7618–7622. [PubMed: 3584132]

13. Saari JC, and Bredberg L (1982). Enzymatic reduction of 11-cis-retinal bound to cellular retinal-binding protein. Biochim. Biophys. Acta 716, 266–272. 10.1016/0304-4165(82)90277-x. [PubMed: 7046808]

14. Stecher H, Gelb MH, Saari JC, and Palczewski K (1999). Preferential release of 11-cis-retinol from retinal pigment epithelial cells in the presence of cellular retinaldehyde-binding protein. J. Biol. Chem. 274, 8577–8585. [PubMed: 10085092]

15. Huang J, Possin DE, and Saari JC (2009). Localizations of visual cycle components in retinal pigment epithelium. Mol. Vis. 15, 223–234. [PubMed: 19180257]

16. Katsanis N, Shroyer NF, Lewis RA, Cavender JC, Al-Rajhi AA, Jabak M, and Lupski JR (2001). Fundus albipunctatus and retinitis punctata albescens in a pedigree with an R150Q mutation in RLBP1. Clin. Genet. 59, 424–429. 10.1034/j.1399-0004.2001.590607.x. [PubMed: 11453974]

17. Maw MA, Kennedy B, Knight A, Bridges R, Roth KE, Mani EJ, Mukkadan JK, Nancarrow D, Crabb JW, and Denton MJ (1997). Mutation of the gene encoding cellular retinaldehyde-binding protein in autosomal recessive retinitis pigmentosa. Nat. Genet. 17, 198–200. 10.1038/ng1097-198. [PubMed: 9326942]

18. Lima de Carvalho JR Jr., Kim HJ, Ueda K, Zhao J, Owji AP, Yang T, Tsang SH, and Sparrow JR (2020). Effects of deficiency in the RLBP1-encoded visual cycle protein CRALBP on visual dysfunction in humans and mice. J. Biol. Chem. 295, 6767–6780. 10.1074/jbc.RA120.012695. [PubMed: 32188692]

19. Saari JC, Nawrot M, Kennedy BN, Garwin GG, Hurley JB, Huang J, Possin DE, and Crabb JW (2001). Visual cycle impairment in cellular retinaldehyde binding protein (CRALBP) knockout mice results in delayed dark adaptation. Neuron 29, 739–748. S0896-6273(01)00248-3 [pii]. [PubMed: 11301032]

20. Xue Y, Shen SQ, Jui J, Rupp AC, Byrne LC, Hattar S, Flannery JG, Corbo JC, and Kefalov VJ (2015). CRALBP supports the mammalian retinal visual cycle and cone vision. J. Clin. Invest. 125, 727–738. 79651 [pii]10.1172/JCI79651. [PubMed: 25607845]

21. Fleisch VC, Schonthaler HB, von Lintig J, and Neuhauss SC (2008). Subfunctionalization of a retinoid-binding protein provides evidence for two parallel visual cycles in the cone-dominant zebrafish retina. J. Neurosci. 28, 8208–8216. [PubMed: 18701683]

22. Schlegel DK, Ramkumar S, von Lintig J, and Neuhauss SC (2021). Disturbed retinoid metabolism upon loss of rlbp1a impairs cone function and leads to subretinal lipid deposits and photoreceptor degeneration in the zebrafish retina. Elife 10, e71473. 10.7554/eLife.71473. [PubMed: 34668483]

23. Collery R, McLoughlin S, Vendrell V, Finnegan J, Crabb JW, Saari JC, and Kennedy BN (2008). Duplication and divergence of zebrafish CRALBP genes uncovers novel role for RPE- and Muller-CRALBP in cone vision. Invest. Ophthalmol. Vis. Sci. 49, 3812–3820. 10.1167/iovs.08-1957. [PubMed: 18502992]

24. de Melo J, Miki K, Rattner A, Smallwood P, Zibetti C, Hirokawa K, Monuki ES, Campochiaro PA, and Blackshaw S (2012). Injury-independent induction of reactive gliosis in retina by loss of

function of the LIM homeodomain transcription factor Lhx2. Proc. Natl. Acad. Sci. U. S. A. 109, 4657–4662. 10.1073/pnas.1107488109. [PubMed: 22393024]

25. Choi EH, Suh S, Einstein DE, Leinonen H, Dong Z, Rao SR, Fliesler SJ, Blackshaw S, Yu M, Peachey NS, et al. (2021). An inducible Cre mouse for studying roles of the RPE in retinal physiology and disease. JCI Insight 6, e146604. 10.1172/jci.insight.146604. [PubMed: 33784255]
26. Kolesnikov AV, Kiser PD, Palczewski K, and Kefalov VJ (2021). Function of mammalian M-cones depends on the level of CRALBP in Muller cells. J. Gen. Physiol. 153, e202012675. 10.1085/jgp.202012675. [PubMed: 33216847]
27. Saari JC, Garwin GG, Van Hooser JP, and Palczewski K (1998). Reduction of all-trans-retinal limits regeneration of visual pigment in mice. Vision Res. 38, 1325–1333. [PubMed: 9667000]
28. Wenzel A, Oberhauser V, Pugh EN Jr., Lamb TD, Grimm C, Samardzija M, Fahl E, Seeliger MW, Reme CE, and von Lintig J (2005). The retinal G protein-coupled receptor (RGR) enhances isomerohydrolase activity independent of light. J. Biol. Chem. 280, 29874–29884. M503603200 [pii] 10.1074/jbc.M503603200. [PubMed: 15961402]
29. Lamb TD, and Pugh EN Jr. (2004). Dark adaptation and the retinoid cycle of vision. Prog. Retin. Eye Res. 23, 307–380. 10.1016/j.preteyeres.2004.03.001S1350946204000151 [pii]. [PubMed: 15177205]
30. Wenzel A, Reme CE, Williams TP, Hafezi F, and Grimm C (2001). The Rpe65 Leu450Met variation increases retinal resistance against light-induced degeneration by slowing rhodopsin regeneration. J. Neurosci. 21, 53–58. 21/1/53 [pii]. [PubMed: 11150319]
31. Lyubarsky AL, Savchenko AB, Morocco SB, Daniele LL, Redmond TM, and Pugh EN Jr. (2005). Mole quantity of RPE65 and its productivity in the generation of 11-cis-retinal from retinyl esters in the living mouse eye. Biochemistry 44, 9880–9888. 10.1021/bi0505363. [PubMed: 16026160]
32. Grimm C, Wenzel A, Hafezi F, Yu S, Redmond TM, and Reme CE (2000). Protection of Rpe65-deficient mice identifies rhodopsin as a mediator of light-induced retinal degeneration. Nat. Genet. 25, 63–66. 10.1038/75614. [PubMed: 10802658]
33. Calvert PD, Krasnoperova NV, Lyubarsky AL, Isayama T, Nicolo M, Kosaras B, Wong G, Gannon KS, Margolskee RF, Sidman RL, et al. (2000). Phototransduction in transgenic mice after targeted deletion of the rod transducin alpha -subunit. Proc. Natl. Acad. Sci. U. S. A. 97, 13913–13918. 10.1073/pnas.250478897. [PubMed: 11095744]
34. Tworak A, Kolesnikov AV, Hong JD, Choi EH, Luu JC, Palczewska G, Dong Z, Lewandowski D, Brooks MJ, Campello L, et al. (2023). Rapid RGR-dependent visual pigment recycling is mediated by the RPE and specialized Muller glia. Cell Rep. 42, 112982. 10.1016/j.celrep.2023.112982. [PubMed: 37585292]
35. Kiser PD, Zhang J, Sharma A, Angueyra JM, Kolesnikov AV, Badiee M, Tochtrop GP, Kinoshita J, Peachey NS, Li W, et al. (2018). Retinoid isomerase inhibitors impair but do not block mammalian cone photoreceptor function. J. Gen. Physiol. 150, 571–590. 10.1085/jgp.201711815. [PubMed: 29500274]
36. Saari JC, and Bredberg DL (1988). Purification of cellular retinaldehyde-binding protein from bovine retina and retinal pigment epithelium. Exp. Eye Res. 46, 569–578. [PubMed: 2838311]
37. Stubbs GW, Saari JC, and Futterman S (1979). 11-cis-Retinal-binding protein from bovine retina. Isolation and partial characterization. J. Biol. Chem. 254, 8529–8533. [PubMed: 468840]
38. Daniele LL, Insinna C, Chance R, Wang J, Nikonov SS, and Pugh EN Jr. (2011). A mouse M-opsin monochromat: retinal cone photoreceptors have increased M-opsin expression when S-opsin is knocked out. Vision Res. 51, 447–458. 10.1016/j.visres.2010.12.017. [PubMed: 21219924]
39. Hood DC, and Hock PA (1973). Recovery of cone receptor activity in the frog's isolated retina. Vision Res. 13, 1943–1951. 10.1016/0042-6989(73)90065-5. [PubMed: 4542882]
40. Arshavsky V (2002). Like night and day: rods and cones have different pigment regeneration pathways. Neuron 36, 1–3. 10.1016/s0896-6273(02)00937-6. [PubMed: 12367498]
41. Babino D, Perkins BD, Kindermann A, Oberhauser V, and von Lintig J (2015). The role of 11-cis-retinyl esters in vertebrate cone vision. FASEB J. 29, 216–226. 10.1096/fj.14-261693. [PubMed: 25326538]

42. Wenzel A, von Lintig J, Oberhauser V, Tanimoto N, Grimm C, and Seeliger MW (2007). RPE65 is essential for the function of cone photoreceptors in NRL-deficient mice. Invest. Ophthalmol. Vis. Sci. 48, 534–542. 10.1167/iovs.06-0652. [PubMed: 17251447]
43. Saari JC, and Crabb JW (2005). Focus on molecules: cellular retinaldehyde-binding protein (CRALBP). Exp. Eye Res. 81, 245–246. S0014-4835(05)00189-2 [pii]10.1016/j.exer.2005.06.015. [PubMed: 16085009]
44. Winston A, and Rando RR (1998). Regulation of isomerohydrolase activity in the visual cycle. Biochemistry 37, 2044–2050. 10.1021/bi971908d. [PubMed: 9485331]
45. Zhao X, Pack W, Khan NW, and Wong KY (2016). Prolonged Inner Retinal Photoreception Depends on the Visual Retinoid Cycle. J. Neurosci. 36, 4209–4217. 10.1523/JNEUROSCI.2629-14.2016. [PubMed: 27076420]
46. Russell S, Bennett J, Wellman JA, Chung DC, Yu ZF, Tillman A, Wittes J, Pappas J, Elci O, McCague S, et al. (2017). Efficacy and safety of voretigene neparvovec (AAV2-hRPE65v2) in patients with RPE65-mediated inherited retinal dystrophy: a randomised, controlled, open-label, phase 3 trial. Lancet 390, 849–860. 10.1016/S0140-6736(17)31868-8. [PubMed: 28712537]
47. Mattapallil MJ, Wawrousek EF, Chan CC, Zhao H, Roychoudhury J, Ferguson TA, and Caspi RR (2012). The Rd8 mutation of the Crb1 gene is present in vendor lines of C57BL/6N mice and embryonic stem cells, and confounds ocular induced mutant phenotypes. Invest. Ophthalmol. Vis. Sci. 53, 2921–2927. 10.1167/iovs.12-9662. [PubMed: 22447858]
48. Mahroo OA, and Lamb TD (2004). Recovery of the human photopic electroretinogram after bleaching exposures: estimation of pigment regeneration kinetics. J. Physiol. 554, 417–437. 10.1113/jphysiol.2003.051250. [PubMed: 14594984]
49. Golczak M, Kiser PD, Lodowski DT, Maeda A, and Palczewski K (2010). Importance of membrane structural integrity for RPE65 retinoid isomerization activity. J. Biol. Chem. 285, 9667–9682. M109.063941 [pii] 10.1074/jbc.M109.063941. [PubMed: 20100834]
50. Schneider CA, Rasband WS, and Eliceiri KW (2012). NIH Image to ImageJ: 25 years of image analysis. Nat. Methods 9, 671–675. 10.1038/nmeth.2089. [PubMed: 22930834]
51. Lewandowski D, Foik AT, Smidak R, Choi EH, Zhang J, Hoang T, Tworak A, Suh S, Leinonen H, Dong Z, et al. (2022). Inhibition of ceramide accumulation in AdipoR1−/− mice increases photoreceptor survival and improves vision. JCI Insight 7, e156301. 10.1172/jci.insight.156301. [PubMed: 35015730]
52. Luu JC, Saadane A, Leinonen H, Choi EH, Gao F, Lewandowski D, Halabi M, Sander CL, Wu A, Wang JM, et al. (2023). Stress resilience-enhancing drugs preserve tissue structure and function in degenerating retina via phosphodiesterase inhibition. Proc. Natl. Acad. Sci. U. S. A. 120, e2221045120. 10.1073/pnas.2221045120. [PubMed: 37126699]
53. Motulsky HJ, and Brown RE (2006). Detecting outliers when fitting data with nonlinear regression - a new method based on robust nonlinear regression and the false discovery rate. BMC Bioinformatics 7, 123. 10.1186/1471-2105-7-123. [PubMed: 16526949]

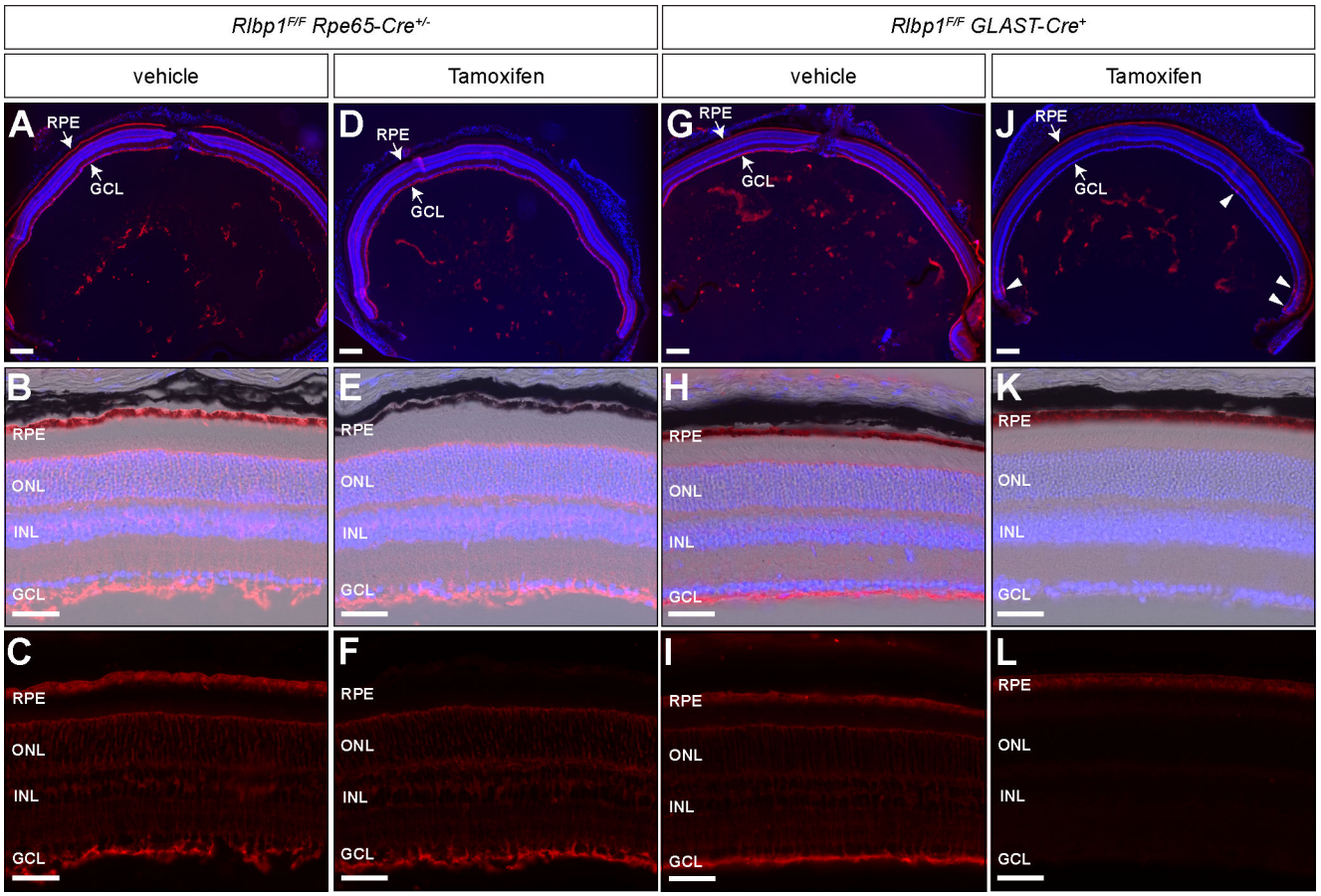

Figure 1. Cell-specific CRALBP knockout in the RPE and MG.

(A-C) Micrographs of a retinal cryo-section obtained from a vehicle-treated *Rlbp1*$^{F/F}$ *Rpe65-Cre*$^{+/-}$ mouse. Red fluorescence within the retinal regions in each panel represents CRALBP immunostaining. The upper panel shows DAPI co-staining of cellular nuclei (blue fluorescence), the middle panel shows CRALBP immunofluorescence and DAPI staining superposed on the corresponding brightfield image, and the bottom panel shows CRALBP immunofluorescence signal only.

(D-F) Micrograph of retinal cryo-sections obtained from a tamoxifen-treated *Rlbp1*$^{F/F}$ *Rpe65-Cre*$^{+/-}$ mouse. Coloring is as described for panels A-C.

(G-I) Micrographs of a retinal cryo-section obtained from a vehicle-treated *Rlbp1*$^{F/F}$ *GLAST-Cre*$^{+}$ mouse. The coloring is as described for panels A-C.

(J-L) Micrographs of a retinal cryo-section obtained from a tamoxifen-treated *Rlbp1*$^{F/F}$ *GLAST-Cre*$^{+}$ mouse. The coloring is as described for panels A-C. The white arrowheads in panel G point to rare MG that maintain CRALBP despite the tamoxifen treatment.

The mice used for this experiment were 3–4-months-old. Tamoxifen was administered by IP injection for the Rpe65-Cre animals and in chow diet for *GLAST-Cre* animals. Scale bars for the low-magnification (top) and high-magnification (middle and bottom) panels represent 200 μm and 50 μm, respectively. The images are representative of three independent experiments. GCL – ganglion cell layer, INL – inner nuclear layer, ONL – outer nuclear layer, RPE – retinal pigment epithelium. See also Figure S2.

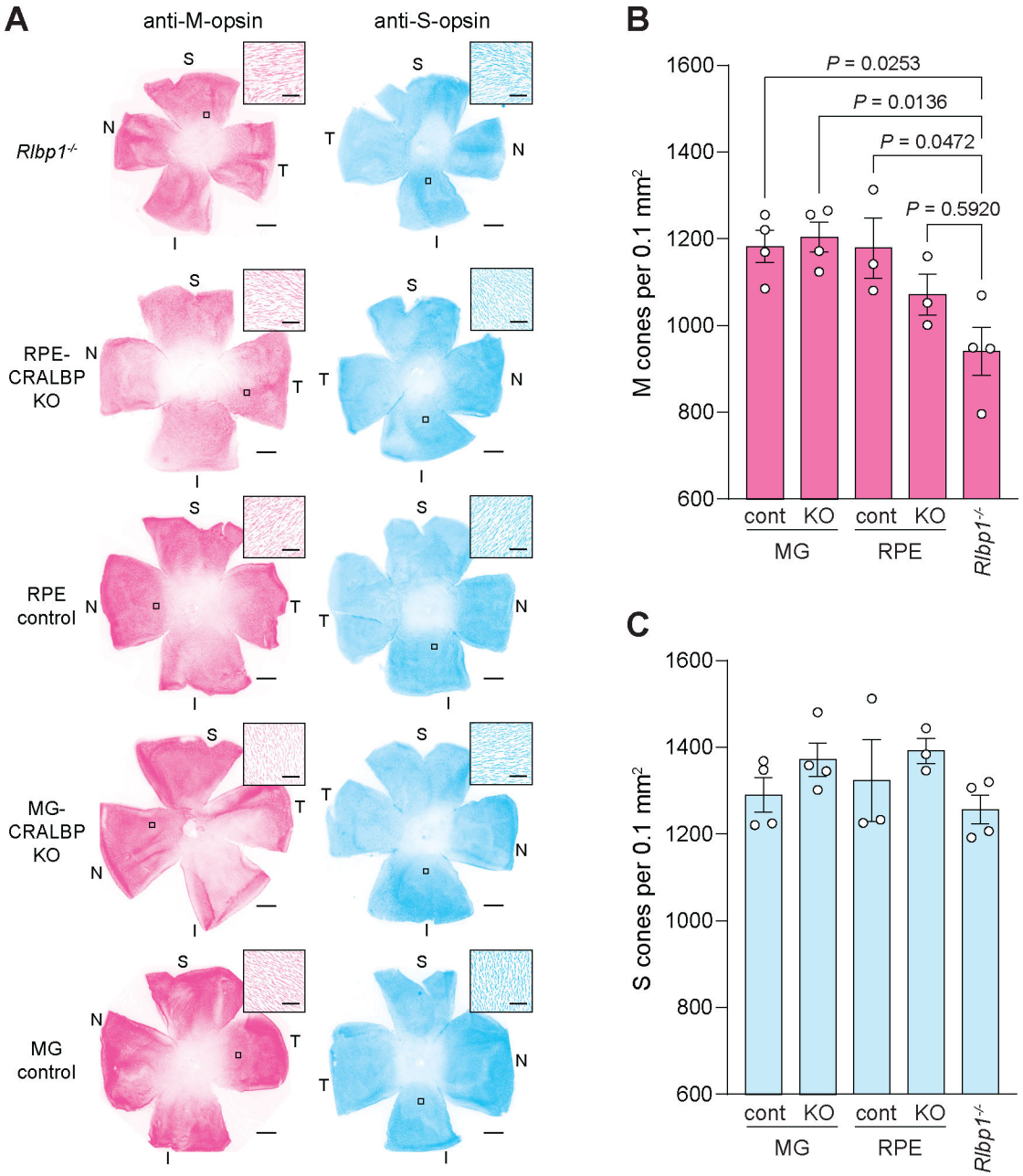

Figure 2. M- and S-cone photoreceptor densities are preserved in cell-specific CRALBP knockout mouse retinas.

(A) Representative whole retina flatmounts from the indicated strains were stained with antibodies recognizing M-cone opsin (left, pink) or S-cone opsin (right, blue) and then imaged by fluorescence microscopy. The superior (S), inferior (I), nasal (N), and temporal (T) quadrants are labeled in each image. Insets, taken from the areas specified by black squares, display the single-cell resolution of the images. Scale bars in the full-scale and inset images represent 500 μm and 50 μm, respectively.

(B) Quantification of M-cone photoreceptor density from retinal flatmount images. One-way ANOVA showed a significant difference among the groups [$F_{(4,13)} = 5.610$, $P = 0.0075$].

Post-hoc analysis with Šídák's multiple comparison test showed significant differences between *Rlbp1*$^{-/-}$ mice and MG control ($P = 0.0253$), MG-CRALBP KO ($P = 0.0136$), and RPE control ($P = 0.0472$) mice.

(C) Quantification of S-cone photoreceptor density from retinal flatmount images. One-way ANOVA did not show a significant difference among the groups [$F_{(4,13)} = 1.374$, $P = 0.2964$].

The mice used for this experiment were 3–5-months-old and on a wild-type background except for *Rlbp1*$^{-/-}$ mice, which were on a *Gnat1*$^{-/-}$ background. CRALBP KO was induced with the tamoxifen chow regimen. In panels B and C, bars represent means, error bars represent SEM, and circles represent biologically independent replicates (n). See also Figures S3 and S4.

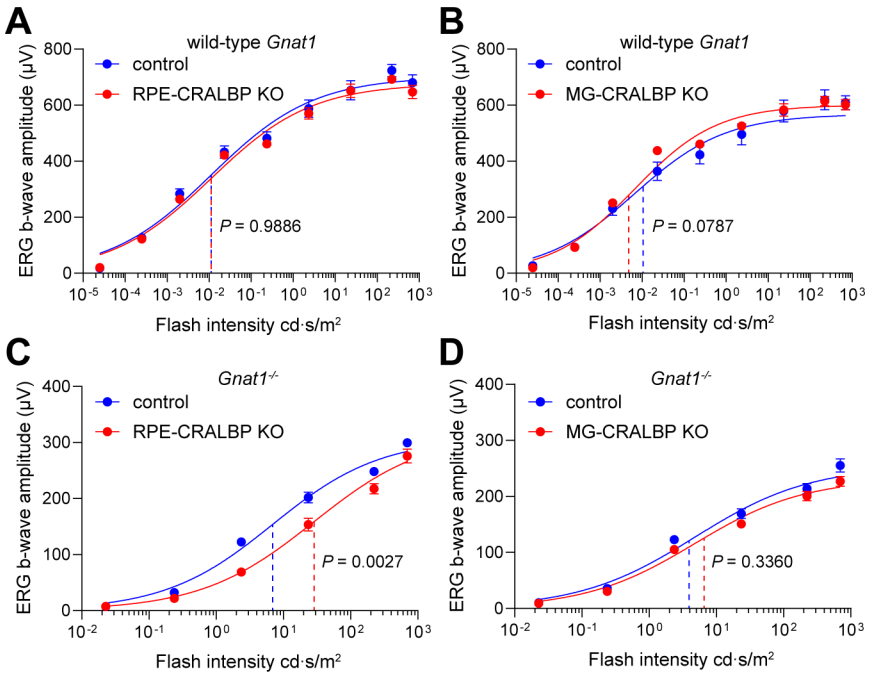

Figure 3. Dark-adapted M-cone ERG b-wave responses are impaired in RPE-CRALBP KO mice

(A) Averaged ERG b-wave intensity-response functions for RPE-CRALBP KO mice (n = 12 eyes) or age/genotype-matched controls (n = 12 eyes) on a wild-type *Gnat1* background. $I_{1/2}$ values (indicated by dashed vertical lines) for RPE-CRALBP KO mice (0.01120 cd·s/m^2) and age-/genotype-matched control mice (0.01127 cd·s/m^2) were not significantly different [$F_{(1,208)} = 0.0002$, $P = 0.9886$].

(B) Averaged ERG b-wave intensity-response functions for MG-CRALBP KO mice (n = 12 eyes) or age/genotype-matched controls (n = 12 eyes) on a wild-type *Gnat1* background. $I_{1/2}$ values (indicated by dashed vertical lines) for MG-CRALBP KO mice (0.00479 cd·s/m^2) and age-/genotype-matched control mice (0.01062 cd·s/m^2) were not significantly different [$F_{(1,206)} = 3.122$, $P = 0.0787$].

(C) Averaged cone ERG b-wave intensity-response functions for RPE-CRALBP KO mice (n = 10 eyes) or age/genotype-matched controls (n = 12 eyes) on a *Gnat1*$^{-/-}$ background. $I_{1/2}$ values (indicated by dashed vertical lines) for RPE-CRALBP KO mice (28.6 cd·s/m^2) and age-/genotype-matched control mice (6.9 cd·s/m^2) were significantly different [$F_{(1,119)} = 9.415$, $P = 0.0027$].

(D) Averaged cone ERG b-wave intensity-response functions for MG-CRALBP KO mice (n = 12 eyes) or age/genotype-matched controls (n = 18 eyes) on a *Gnat1*$^{-/-}$ background. $I_{1/2}$ values (indicated by dashed vertical lines) for MG-CRALBP KO mice (6.6 cd·s/m^2) and age-/genotype-matched control mice (3.9 cd·s/m^2) were not significantly different [$F_{(1,172)} = 0.9308$, $P = 0.3360$].

The mice used for this experiment were 3–4-months-old and had been dark-adapted for 48 h (panels A and B) or 24 h (panels C and D) before ERG recordings. RPE-CRALBP KO and MG-CRALBP KO were induced with the IP tamoxifen and chow tamoxifen regimens, respectively. Data points represent mean values and error bars represent SEM. Curves

represent the best fits of the Naka-Rushton equation to the data. Statistical comparisons of $I_{1/2}$ values were performed with the extra sum-of-squares F test. See also Figure S5.

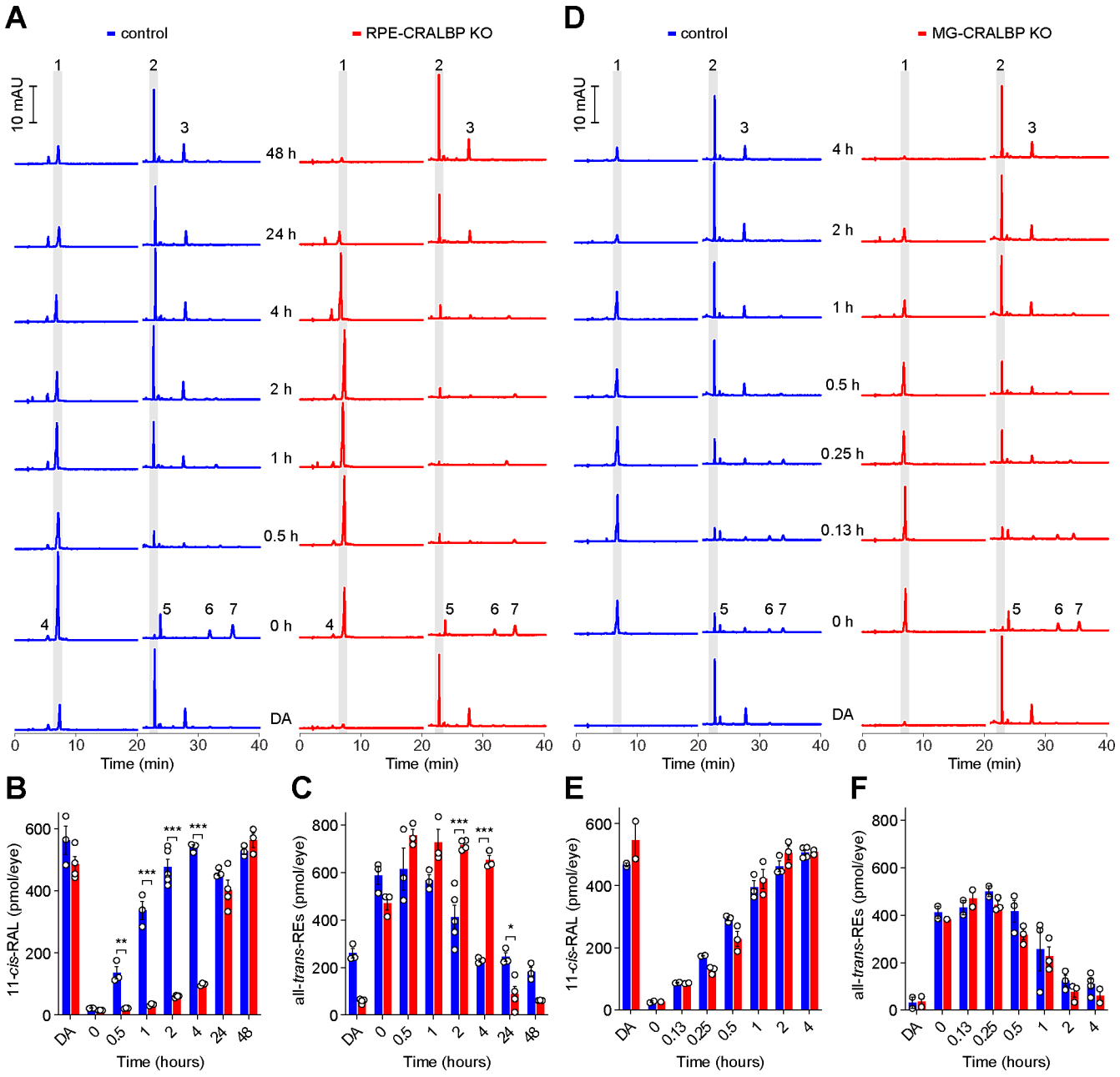

Figure 4. Visual cycle retinoid metabolism is perturbed in RPE-CRALBP KO mice

(A) Representative HPLC chromatograms showing extracted ocular retinoids from control and RPE-CRALBP KO mice in a pre-bleach, dark-adapted (DA) state as well as at various times after a bright-light exposure that bleached ~95% of the retinal visual pigment. The chromatograms represent absorbance at 325 nm. Peak identities are as follows: 1 – all-*trans*-retinyl esters, 2 – *syn*-11-*cis*-retinal oxime, 3 – *anti*-11-*cis*-retinal oxime, 4 – 11-cis-retinyl ester, 5 – *syn*-all-*trans*-retinal oxime, 6 – *anti*-all-*trans*-retinal oxime, 7 – all-*trans*-retinol. (B) Quantification of 11-*cis*-RAL showed a marked delay in visual pigment recovery following the bleaching light exposure in RPE-CRALBP KO mice as compared to controls. There was a significant effect of RPE-CRALBP KO on the time-dependent recovery of

11-*cis*-RAL [$F_{(1, 32)} = 326$, $P < 0.0001$]. Post-hoc analysis showed significant differences between the two groups at the 0.5, 1, 2, and 4 h time points (** $P = 0.0020$; *** $P < 0.0001$).
(C) Quantification of all-*trans*-REs showed a marked delay in their clearance following the bleaching light exposure in RPE-CRALBP KO mice as compared to controls. There was a significant effect of RPE-CRALBP KO on the time-dependent clearance of all-*trans*-RE levels [$F_{(1, 32)} = 18.89$, $P = 0.0001$]. Post-hoc analysis showed significant differences between the two groups at the 2, 4, and 24 h time points (* $P = 0.0405$; *** $P < 0.0001$).
(D) Representative HPLC chromatograms showed extracted ocular retinoids from control and MG-CRALBP KO mice in a pre-bleach, dark-adapted (DA) state as well as at various times after a bright-light exposure that bleached ~95% of the retinal visual pigment. The chromatograms represent absorbance at 325 nm.
(E) Quantification of 11-*cis*-RAL showed comparable visual pigment recovery following the bleaching light exposure between MG-CRALBP KO mice and controls. There was no significant effect of RPE-CRALBP KO on 11-*cis*-RAL recovery [$F_{(1, 22)} = 0.3370$, $P = 0.5675$].
(F) Quantification of all-*trans*-REs showed similar clearance following the bleaching light exposure between RPE-CRALBP KO mice and controls. There was no significant effect of RPE-CRALBP KO on all-*trans*-RE recovery [$F_{(1, 22)} = 2.755$, $P = 0.1111$].
Three to four-month-old mice that were treated with IP tamoxifen or oil vehicle were used for these experiments. Bars represent means, error bars represent SEM, and circles represent biologically independent replicates. Data were analyzed by repeated measures, two-way ANOVA followed by Šídák's multiple comparison test. Peak identities were assigned by comparison of their retention times and absorbance spectra to authentic standards. See also Figures S6 and S7 and Tables S2 and S3.

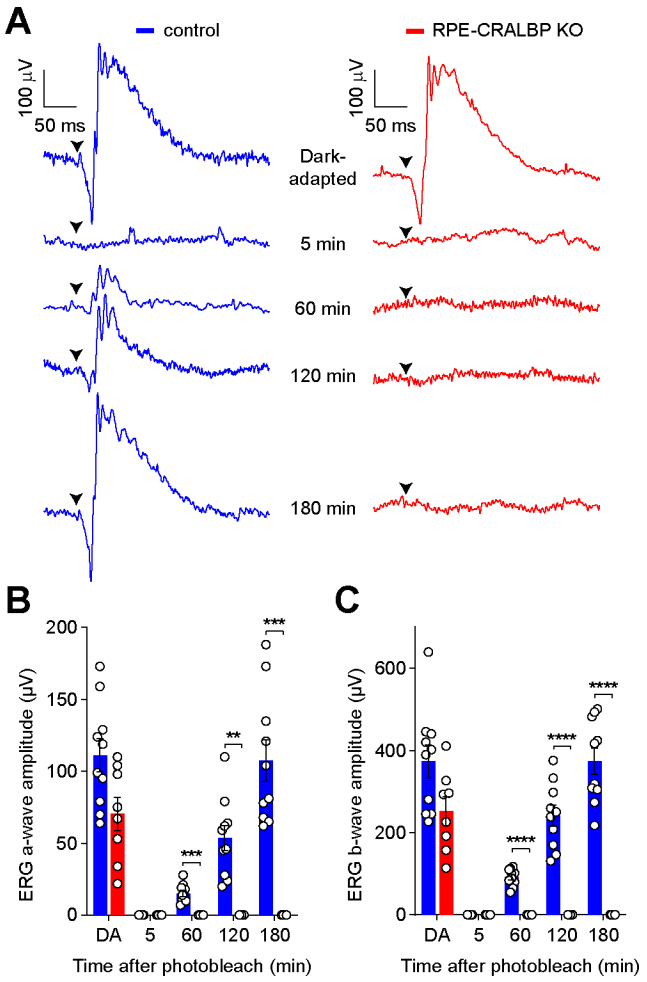

Figure 5. RPE-CRALBP KO mice exhibit profoundly delayed rod dark adaptation.

(A) Representative scotopic ERG traces obtained from RPE-CRALBP KO (red) and age- and genotype-matched control mice (blue) in the overnight dark-adapted (DA) state and after various periods of dark-adaptation following a bright light exposure that bleached ~95% of visual pigment. The ERG responses were initiated with a 0.1 cd·s/m^2 flash of light (black arrowheads), which exclusively simulates rod responses.

(B) Quantification of the ERG a-wave responses after the indicated periods of dark adaptation. There was a significant effect of RPE-CRALBP knockout on ERG a-wave recovery [$F_{(1,16)}$ = 49.44, P < 0.0001]. Post-hoc analysis showed significant differences between the two groups at the 60-, 120-, and 180-min time points (** P = 0.0007; *** P = 0.0002). Control mice, n = 10 eyes; RPE-CRALBP KO mice, n = 8 eyes.

(C) Quantification of the ERG b-wave responses after the indicated periods of dark adaptation. There was a significant effect of RPE-CRALBP knockout on ERG b-wave recovery [$F_{(1,16)}$ = 136.9, P < 0.0001]. Post-hoc analysis showed significant differences between the two groups at the 60-, 120-, and 180-min time points (*** P < 0.0001). Control mice, n = 10 eyes; RPE-CRALBP KO mice, n = 8 eyes.

The mice used for this experiment were 4-months-old and on a wild-type *Gnat1* background. RPE-CRALBP KO was achieved with tamoxifen chow administration. Bars represent

means, error bars represent SEM, and circles represent individual replicates. Statistical analysis was performed by repeated-measures, two-way ANOVA followed by Šídák's multiple comparison test.

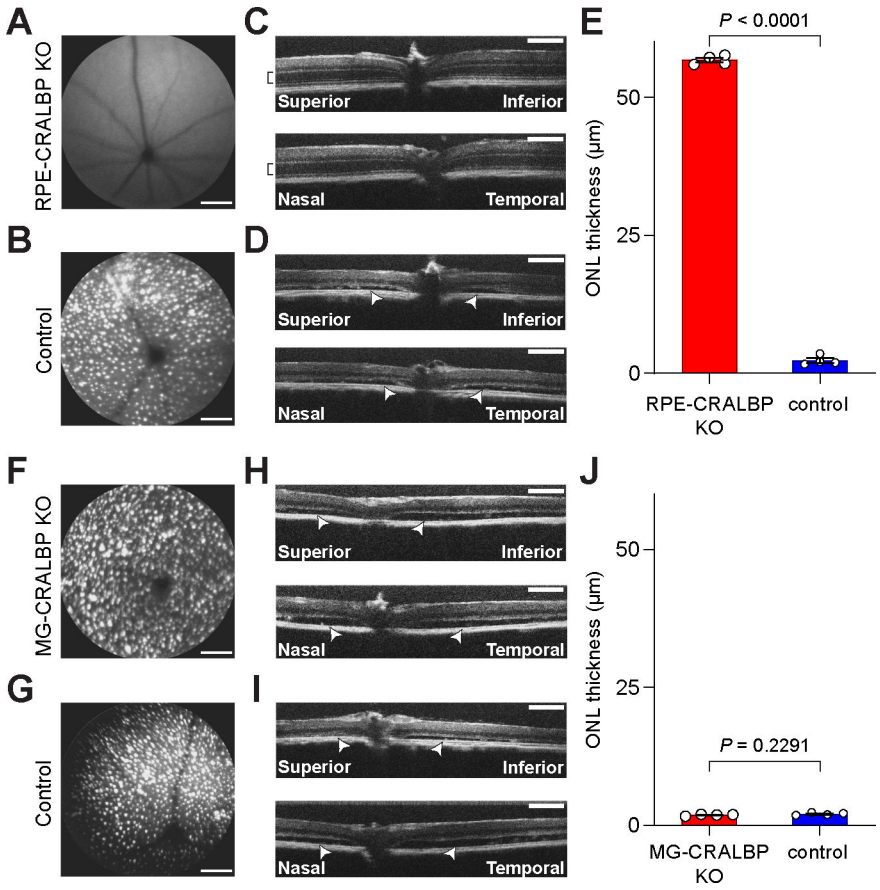

Figure 6. RPE-CRALBP KO mice are resistant to acute retinal damage induced by bright light.

(A, B) *In vivo* scanning laser ophthalmoscopy (SLO) images showing retinal autofluorescence in RPE-CRALBP KO mice and age/genotype-matched controls that were exposed to 15,000 lux illumination for 8 h. The white puncta observed in the control mouse image signifies inflammatory changes in the retina. The images are representative of n = 4 biological replicates.

(C, D) *In vivo* retinal optical coherence tomography (OCT) images from RPE-CRALBP KO mice and age/genotype-matched controls that were exposed to 15,000 lux illumination for 8 h. An intact outer nuclear layer (ONL, black brackets) is observed for the RPE-CRALBP KO mice while control animals exhibited near-complete loss of the ONL as well as retinal detachment (white arrowheads), both of which signify retinal phototoxicity. These images are representative of n = 4 biological replicates.

(E) Quantification of the retinal ONL thickness as measured by OCT shows a severe reduction in thickness for control animals as compared to RPE-CRALBP KO mice, which exhibited normal ONL thickness. The bars represent means, the error bars represent SEM, and the circles represent biological replicates (n = 4 mice for each group). An unpaired, two-tailed Student's t-test showed a significant difference between the sample means ($P < 0.0001$).

(F, G) *In vivo* SLO images showing retinal autofluorescence in MG-CRALBP KO mice and age/genotype-matched controls that were exposed to 15,000 lux illumination for 8 h. The

white puncta observed in both types of mice signifies inflammatory changes in the retina. The images are representative of n = 4 biological replicates.

(H, I) *In vivo* retinal OCT images from RPE-CRALBP KO mice and age/genotype-matched controls that were exposed to 15,000 lux illumination for 8 h. Both MG-CRALBP KO mice and control mice exhibited near-complete loss of the ONL as well as retinal detachment (white arrowheads), both of which signify retinal phototoxicity. These images are representative of n = 4 biological replicates.

(J) Quantification of the retinal ONL thickness as measured by OCT shows a severe reduction in ONL in both MG-CRALBP KO and control animals. The bars represent means, the error bars represent SEM, and the circles represent biological replicates (n = 4 for each group). An unpaired, two-tailed Student's t-test showed sample means were not significantly different ($P = 0.2291$).

Three to five-month-old mice were used for this experiment. RPE-CRALBP KO and MG-CRALBP KO were induced by administration of tamoxifen chow. SD-OCT images (B-scans) were recorded one week after the bright-light exposure. The scale bars in panels A, B, F, and G represent 500 μm. The scale bars in panels C, D, H, and I represent 200 μm.

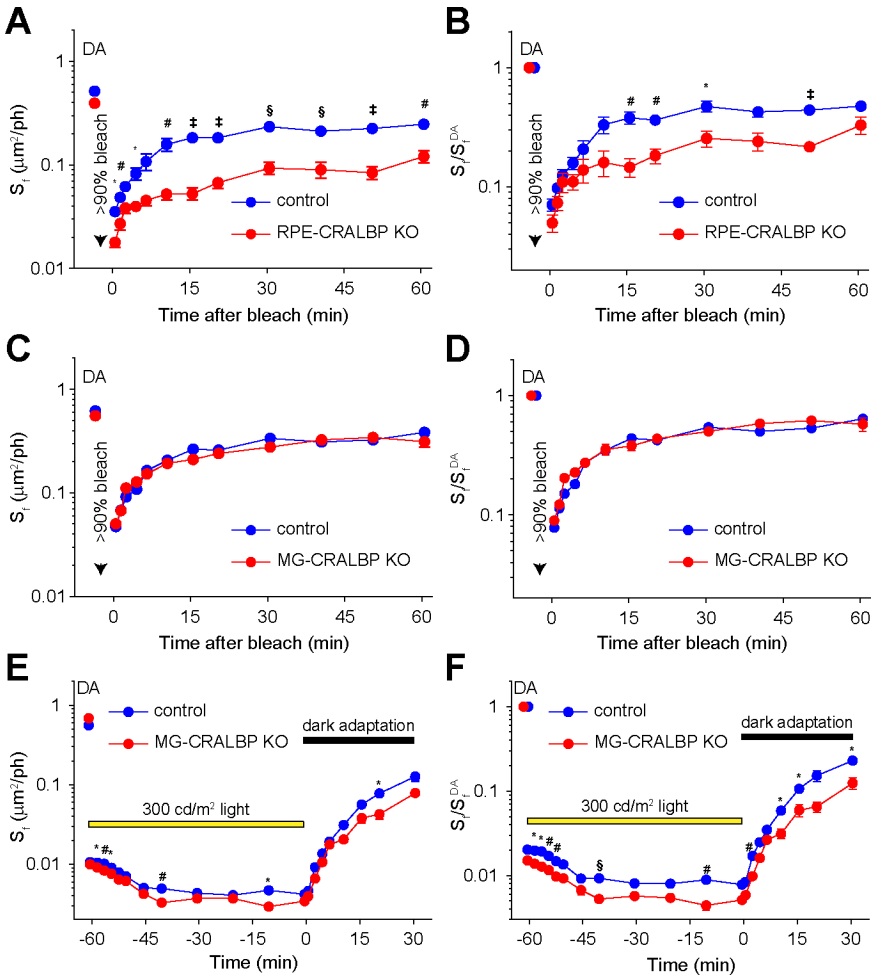

Figure 7. RPE-CRALBP KO impacts M-cone dark adaptation to a greater extent than MG-CRALBP KO.

(A) Time-dependent recovery of the raw ERG b-wave sensitivity in RPE-CRALBP KO mice (n = 10 eyes) or age/genotype-matched controls (n = 12 eyes) after a 35-s exposure to intense 520 nm LED light that bleached > 90% of M-cone visual pigment. There was a significant effect of RPE-CRALBP knockout on cone ERG b-wave recovery [$F_{(1,20)} = 87.41$, $P < 0.0001$]. Post-hoc analysis showed sensitivity reductions at the indicated data points with the following significance levels: $^{*}P < 0.05$, $^{\#}P < 0.01$, $^{\S}P < 0.001$, and $^{\ddagger}P < 0.0001$.

(B) The data in panel A were normalized to their own S_f^{DA} and replotted. The effect of RPE-CRALBP knockout remained significant [$F_{(1,20)} = 21.33$, $P = 0.0002$]. Post-hoc analysis showed sensitivity reductions at the indicated data points with the following significance levels: $^{*}P < 0.05$, $^{\#}P < 0.01$, and $^{\ddagger}P < 0.0001$.

(C) Time-dependent recovery of the raw ERG b-wave sensitivity in MG-CRALBP KO mice (n = 12 eyes) or age/genotype-matched controls (n = 18 eyes) after a 35-s exposure to intense 520 nm LED light that bleached > 90% of M-cone visual pigment. There was no significant effect of MG-CRALBP knockout on cone ERG b-wave recovery [$F_{(1,28)} = 1.083$, $P = 0.3069$].

(D) The data in panel C were normalized to their own S_f^{DA} and replotted. The effect of MG-CRALBP knockout remained non-significant [$F_{(1,28)} = 0.3032$, $P = 0.5862$].
(E) Time-dependent changes in the raw cone-driven ERG b-wave sensitivity in MG-CRALBP KO mice (n = 14 eyes) and age/genotype-matched controls (n = 12 eyes) during a 1-h 300 cd/m^2 light exposure followed by a recovery period in the dark. There was a significant effect of MG-CRALBP knockout on cone ERG b-wave sensitivity [$F_{(1,24)} = 12.86$, $P = 0.0015$]. Post-hoc analysis showed sensitivity reductions at the indicated data points with the following significance levels: $^{*}P < 0.05$, $^{\#}P < 0.01$.
(F) The data in panel E were normalized to their own S_f^{DA} and replotted. The effect of MG-CRALBP knockout remained significant [$F_{(1,24)} = 17.73$, $P = 0.0003$]. Post-hoc analysis showed sensitivity reductions at the indicated data points with the following significance levels: $^{*}P < 0.05$, $^{\#}P < 0.01$, and $^{\S}P < 0.001$.
The mice used for this experiment were between 2.5–4-months-old. RPE-CRALBP KO and MG-CRALBP KO were induced with the IP tamoxifen and tamoxifen chow regimens, respectively. For both panels, circles represent means and error bars represent SEM. Statistical analysis was performed by repeated-measures, two-way ANOVA followed by Šídák's multiple comparison test. In some cases, the error bars are smaller than the mean value symbols. See also Figure S8.